**UNIVERSITA' DEGLI STUDI DI TORINO**

DEPARTMENT OF ONCOLOGY

PHD PROGRAM IN MOLECULAR MEDICINE

XXXVI CYCLE

# DECIPHERING THE PATHWAYS AT THE BASIS OF RESISTANCE TO CHEMOTHERAPY, IMMUNE-KILLING AND TARGET THERAPY TO IDENTIFY NEW PHARMACOLOGICAL TOOLS AGAINST LUNG CANCER

THESIS AUTHOR: MARTINA GODEL

SUPERVISORS: CHIARA RIGANTI, JOANNA KOPECKA

PHD PROGRAM COORDINATOR: FRANCESCO NOVELLI

ACADEMIC YEARS OF ENROLLEMENT: 2020-2024

CODE OF SCIENTIFIC DISCIPLINE: BIOS-07/A

# Index

**ABSTRACT**

Non-Small Cell Lung Cancer (NSCLC) is the main cause of cancer-related death in the world. This thesis analyzed the underlying molecular mechanisms of lung cancer chemo-immuno-resistance and target therapy resistance, which still represent a challenge in cancer treatment. Evaluation of the expression of Signal Transducer of Activator of Transcription-1 (STAT1) allowed the choice of three NSCLC cell lines, among six different analyzed, to carry out the experiments. The first part of the thesis investigated the role of STAT1 in resistance to chemotherapy and immune-killing: NSCLC cell viability was reduced due to an increase in cancer cells' chemosensitivity to chemotherapeutics, and an increase in T-lymphocytes proliferation and activation. Moreover, the involvement of paracrine mechanisms in STAT1-dependent therapy resistance was assessed: a differential expression of cytokines was identified, as well as a different proteomic profile in Extracellular Vesicles (EVs) released from wild-type and STAT1-silenced NSCLC cells. Results suggest that STAT1 silencing resensitizes NSCLC cells to cisplatin and paclitaxel-based chemotherapy and immune killing by T-lymphocytes, demonstrating its potential role in mediating resistance through the involvement of paracrine mechanisms. The second part of this work addressed the resistance to epidermal growth factor receptor (EGFR) inhibitors, using erlotinib-sensitive and erlotinib-resistant NSCLC cells. A small library of erlotinib-derivatives containing a ferrocene group was tested, and a panel of top-compounds was identified. These compounds were found to be significantly more effective than erlotinib and independent from classical mechanisms of resistance to EGFR inhibitors. The efficacy of these compounds was due to their ability to release reactive oxygen species (ROS) thanks to the presence of the ferrocene group, resulting in DNA damage, inhibition in G2/M phase of cell cycle, mitochondrial stress and activation of caspase-9 and -3 mediated apoptosis.

# 1. Introduction

## 1.1 Epidemiology and risk factors of lung cancer

Globally, lung cancer is the leading cause of cancer mortality in men and is the second highest cause of cancer death in women, only behind breast cancer. Its mortality rate counts more than 2 million new cases and almost 2 million deaths per year. Lung cancer incidence and mortality are generally twice as high in men as in women, although they vary greatly across different regions of the world, with an overall survival (OS) rate of 50% and a five-year survival rate of 19% in Europe and the US[1].

Tobacco exposure is widely recognized as the main risk factor for lung cancer worldwide. In fact, 80–90 % of lung cancer cases in the world are associated with the carcinogens released in the combustion of tobacco, which impacts many organs but lungs the most[2]. The link between tobacco consumption and lung cancer was recognized as early as the 1930s through epidemiological case–control studies, and polycyclic aromatic hydrocarbons present in cigarette smoke were later identified as carcinogens[1]. Today we know that smoke contains high carcinogenic substances such as free radicals, namely quinones and its derivatives inorganic agents like nickel, arsenic, and chromium, as well as polycyclic aromatic hydrocarbons, N-nitrosamines, heterocyclic and aromatic amines, and aldehydes[3]. Second-hand smoke is also a recognized risk factor for lung cancer, as it is estimated to increase the risk of 20–30%, proportionally with the degree of exposure[1].

Many studies have found a link between air pollution and the incidence of lung cancer, as air pollutants include a great quantity of particulate matter (PMs) and gases that can damage the lung, such as $PM_{10}$, $PM_{2.5}$, toxic metals, sulfur oxides, nitrogen oxides, and microorganisms. Indoor air pollutants can also lead to lung cancer, such as cooking fumes and odors from painting[4]. The main mechanisms may involve oxidative stress, inflammation, DNA damage, epigenetic regulation, metabolism, and related signal transduction pathway. For example, ROS production is related to the activation of mitogen-activated protein kinase (MAPK) family members and transcription factors, such as nuclear factor kappa-light-chain-enhancer of activated B cells (NF-κB). NF-κB is a marker of inflammation, and exposure to fine particles induces a significant increase in it. The expression of cytokines, chemokines, and proteins related to autophagy and angiogenesis have been shown to increase *in vitro* and *in vivo*, with the occurrence of acute inflammation[4].

Additionally, mutagens in air pollution seem to induce mutations in EGFR or Kirsten Rat Sarcoma Viral Oncogene (KRAS) genes in lung cells, leading to an increased proliferation, and at the same time they enable macrophage recruitment to release IL-1β, promoting inflammation and cancer developement[5]. Other carcinogenic agents, as stated by the International Agency for Research on Cancer (IARC), are associated with lung cancers: asbestos, silica, arsenic, radon, beryllium, diesel exhaust, nickel, cadmium and chromium[1].

Moreover, a family history of lung cancer is a recognized risk factor for the disease, although the heritability - which refers to the proportion of variance in cancer risk among individuals that can be attributed to genetic differences - is complex and still under investigation. A significant case–control study by the International Lung Cancer Consortium found that individuals with a first-degree relative who has lung cancer bear a 1.51 times higher risk of developing the disease themselves, especially in case of a sibling, even after accounting for smoking and other possible influencing factors[6].

### 1.2 Lung cancer subtypes and staging

Lung cancer is canonically classified into two main types, which differ in their histology and origin: Non-Small Cell Lung Cancer (NSCLC), affecting approximately 85% of patients, and Small Cell Lung Cancer (SCLC)[7].

SCLC, the most aggressive subtype of the two subtypes, accounts for 13–15% of new lung cancer cases, with a 5-year survival rate of patients below 7%. SCLC generally has an aggressive progression characterized by an unstable tumor genome, rapid growth rate, increased angiogenesis, and high metastatic potential. Most patients with SCLC already show metastasis at the moment of diagnosis, followed by a rapid progression and eventual death. SCLC is considered a hard-to-treat cancer type, as targeted treatment against it and survival rate for patients have not improved over the years. Its pre-invasive histological pattern and intrinsic molecular heterogeneity makes early screening ineffective[8].

Platinum-based chemotherapy still is the frontline treatment of SCLC, and most SCLC tumors initially respond well to it but eventually relapse. The standard second-line treatment has consisted of topotecan for years, although with limited efficacy, with a response rate of 25% for platinum-sensitive patients and less than 10% for platinum-resistant or refractory patients. Recently, immune checkpoint inhibitors were introduced as treatment options for SCLC.

However, the efficacy of anticancer immunity in SCLC remains limited mainly because of the low expression of Programmed Death Ligand 1 (PD-L1), which calls for the development of personalized treatments[9].

NSCLC is subdivided into several histological subtypes including adenocarcinoma (LUAD), squamous cell carcinoma (LUSC) and large cell carcinoma (LCC). LUAD and LUSC are the two predominant NSCLC subtypes, respectively representing 50% and 40% of cases. In general, LUAD arises in more distal airways, whereas LUSC arises in more proximal airways and is more strongly associated with smoking and chronic inflammation than LUAD. LUAD often shows glandular histology and expresses biomarkers that are consistent with an origin in the distal lung, including thyroid transcription factor 1 (TTF1) and keratin 7 (KRT7). By contrast, LUSC is characterized by squamous differentiation, which is more reminiscent of the pseudostratified columnar epithelium between the trachea and upper airways. LUSC is distinguished from LUAD in the clinic by immunostaining for cytokeratin 5 and cytokeratin 6 and/or the transcription factors SRY-box 2 (SOX2) and p63. LCC is usually diagnosed by exclusion of the other two, although it is unclear whether large cell carcinomas are genetically distinct from LUAD or LUSC[7,10].

Following the identification of KRAS and V-Raf Murine Sarcoma Viral Oncogene Homolog B (BRAF) mutations, EGFR mutations were discovered in patients with LUAD and were associated with response to EGFR inhibitors. Other mutations and amplifications in many potentially targetable oncogenes have been identified in LUAD since then, including human epidermal growth factor receptor 2 (HER2), MET, fibroblast growth factor receptor 1 (FGFR1) and FGFR2, as well as fusion oncogenes involving anaplastic lymphoma kinase (ALK), the ROS1 receptor tyrosine kinase, neuregulin 1 (NRG1), neurotrophic tyrosine kinase receptor type 1 (NTRK1) and RET1. These oncogenic signatures are present in most of LUAD cases. Instead, mutations in genes such as discoidin domain-containing receptor 2 (DDR2), Fibroblast growth factor receptor 1 (FGFR1), FGFR2, FGFR3 and genes in the hosphatidylinositol-4,5-Bisphosphate 3-Kinase (PI3K) pathway seem to be more common in LUSC, and some of these mutations have been validated by preclinical studies as driver mutations. New Generation Sequencing (NGS) studies have also revealed that the complexity of somatic alterations in NSCLCs also include epigenome modifiers, transcription factors, splicing factors and genes involved in cellular immunity[7].

NSCLC subtyping is fundamental to define the optimal therapy for each case, and so is NSCLC staging. Tumor staging establishes the extent of the primary tumor and the eventual spreading outside the primary site. The TNM system, based on the size of the primary tumor (T), the presence of tumor tissue in lymph nodes (N) and the spread of the tumor out of the primary site (M), determines treatment options and provides information on prognosis and eligibility for clinical trials[11].

### 1.3 Genetic alterations in NSCLC

The most common mutations in NSCLC are found in the following genes: EGFR, ALK, KRAS, BRAF, ROS1, RET, HER2, and MET.

EGFR is a transmembrane receptor tyrosine kinase that belongs to ErbB family of receptors and its mutations, when detected, are usually present in the founder clones, indicating their roles in tumor initiation and representing attractive targets for therapeutic intervention. Main mutations in this gene include exon 19 deletion or point mutation of exon 21, which confer sensitivity to EGFR Tyrosine-Kinase Inhibitors[12].

Younger NSCLC patients commonly bear rearrangement of ALK gene, another member of the receptor tyrosine kinase family that is frequently found to be expressed in the nervous system but not in the lung. However, mutation consisting of the ALK fusion with echinoderm microtubule-associated protein-like 4 (EML4), which increases metastasis, and phenomena correlated with the upregulation of STAT3 are found in lung cancer patients. ALK rearrangements are treated with ALK Inhibitors which result in prolonged progression-free survival (PFS) and OS compared with standard chemotherapy[13].

25% of NSCLC patients wild-type for EGFR and ALK, present Kristen Rat Sarcoma viral oncogene (KRAS) mutations. RAS is one of the members of the RAS superfamily that is activated upon guanosine-5'-triphosphate (GTP) binding, subsequently activates RAS/RAF/MAPK2/MAPK and PI3K/Akt pathways to trigger cell proliferation and survival in both normal and cancer cells. KRAS targeted therapies are selective because they attack the point mutation and don’t affect the wild-type KRAS protein[14].

BRAF kinase is associated with RAS/RAF/MEK/ERK pathway that is activated when BRAF is mutated, resulting in increased cell prolifetation[15]. Mutation V600E of BRAF is related to MAPK pathway activation, so the combination of one BRAF-targeting drug and

another MEK-targeting is currently being evaluated[12]. Other potential targets are represented by gene rearrangements of ROS1, a receptor tyrosine kinase that may have a role in growth or differentiation, and Ret Proto-Oncogene (RET) determining PI3K/AKT and JAK/STAT signaling pathway activation, ultimately leading to cell proliferation, invasion, and migration. Additional targetable mutations are overexpression, amplification, and aberrant activation of HER2, also known as ErbB2, which belongs to the ErbB receptors family, and MET[12,16].

### 1.4 NSCLC treatments

In lung cancer inter-patients, intra- and inter-tumor variability and genetic diversity between the primary lung tumor and corresponding metastatic lesions, reflect an important level of molecular heterogeneity, which leads to patients with the same histotype showing a different response to treatment[17].

Treatments for NSCLC are usually stage-specific. Early stages, namely stage I/stage II, and localized NSCLC can undergo surgical resection, followed by adjuvant therapies to decrease the risk of relapse[18], while locally advanced NSCLC is treated by neoadjuvant therapy, surgery, and adjuvant therapy. Unfortunately, most cases of NSCLC are diagnosed at later stages, when surgery is no longer a suitable option. Patients for whom the surgery is excluded, can be treated with chemotherapy, radiotherapy, immunotherapy, and targeted therapy**.**

In the absence of targeted mutations, NSCLC standard treatment is platinum-based chemotherapy, to which most patients initially respond, although the occurrence of later relapses is frequent. The most used platinum drugs are cisplatin and carboplatin, respectively as first and second-generation drugs[19]. Platinum-based chemotherapy involves passive drug transport into the cancer cells by the cell membrane channel CRT1/2. Cisplatin creates DNA adducts, intra- and inter-strand crosslinks, causing nuclear and mitochondrial DNA damage, blocking DNA replication and transcription, and inducing the production of ROS, leading to cell apoptosis[20]. Other chemotherapeutic drugs include taxanes, such as paclitaxel and docetaxel, which trigger cell cycle arrest by binding to the cytoskeleton[21], gemcitabine, a pyrimidine analog used as first-line treatment for advanced NSCLC, often combined with cisplatin and carboplatin, which is intercalated into DNA strands during S phase of cell cycle and leads to a single-strand break in the molecule[22], and pemetrexed, an antifolate drug which arrests the cells in S phase of cell cycle, inhibiting enzymes involved in pyrimidine and purine

synthesis[23]. For advanced-stage NSCLC, cytotoxic combination chemotherapy is the first-line therapy, which is usually a platinum-based (cisplatin or carboplatin) doublet therapy with paclitaxel, gemcitabine, docetaxel, vinorelbine, irinotecan, or pemetrexed. Studies testing several combinations of cisplatin and other drugs have shown that they have similar efficacy in advanced NSCLC. Consequently, drug combination depends on the nature and frequency of toxic and side effects, and recent clinical trial studies have proven that no single therapeutic regime is significantly superior to the combination regime[24].

Radiotherapy option is used for patients who can't undergo surgical resection, or as palliative care to improve quality of life in NSCLC patients who do not respond to surgery or chemotherapy, as it can create DNA damage and induction of immune response towards cancer cells. A technique called stereotactic body radiation therapy (SBRT) is used for early-stage NSCLC patients who have a single small nodule in the lung without any metastases to nearby lymph nodes. This technique uses an advanced coordinate system to locate the tumor and ensure precise placement of the tracking device, to deliver concentrated and highly focused radiation. New technologies such as 4D tomography, stereotactic body radiotherapy, and intensity-modulated radiotherapy have decreased side effects, and for this reason it can be used for patients without metastases or older patients to improve their quality of life[23,25].

The molecular identification of mutations correlated with NSCLC has allowed the development of several targeted therapies, whose main purpose is to target point mutations and rearrangements on oncogene or abnormal proteins involved in the growth and spread of cancer cells, and to limit damage to healthy cells[12]. Among them, tyrosine kinase inhibitors (TKIs) against mutant EGFR were the first to be developed and used with better outcomes than standard first-line chemotherapy for selected patients with NSCLC, and nowadays, third-generation EGFR TKIs are used in the first-line treatment of patients with EGFR-mutant NSCLC and fourth-generation TKIs are being evaluated in clinical trials. Notable TKIs are gefitinib, erlotinib, cetuximab and panitumumab[26,27]. Following the success of EGFR-targeted therapy, other frequent oncogenic drivers of NSCLC have been explored as therapeutic targets[26], leading to the development of many FDA-approved drugs, such as crizotinib and lorlatinib for ALK-positive or ROS-1-positive NSCLC, pralsetinib and selpercatinib for metastatic RET fusion-positive NSCLC. Other drugs against HER-2, KRAS and BRAF mutations are currently in Phase II clinical trial. Moreover, efforts are being made toward targeting signaling pathways commonly mutated in NSCLC, such as the PI3K/AKT/mTOR and

JAK–STAT pathways, with the generation of inhibitors against PI3K (LY294002), mTOR (temsirolimus, everolimus), JAK2 (ruxolitinib, CYT387), currently under clinical trial[12,27].

Furthermore, the discovery of immune checkpoints and subsequent development of immune checkpoints inhibitors (ICIs) opened to new possibilities the therapeutic landscape of NSCLC. Immunotherapy works by boosting and restoring the immune system's anti-cancer function against tumor-specific antigens, hampering the tumor's immunosuppressor role[23]. Non-specific immunomodulatory therapies, or therapies that are not directed against a specific antigen but aim to boost the immune response, are usually based on IL-2, IFNγ, immune-stimulatory agents such as CpG oligonucleotides, and enzyme inhibitors, and act with direct anti-tumor effects and reverse immunosuppression[28]. ICIs block the tumor evasion from the immune system, hampering the link between immune checkpoint proteins (ICPs) and giving a better response in an inflamed tumor microenvironment (TME), where there is a higher expression of ICPs. Of the several known immune checkpoints utilized by the tumor to evade host immune system, the best known and farthest along in clinical application is programmed cell death protein-1/programmed cell death ligand-1(PD-1/PD-L1) and cytotoxic T lymphocyte antigen-4 (CTLA-4) pathways. Inhibition of these pathways enables priming and anti-tumor activity of cytotoxic T-cells[29].

PD-1 is a receptor expressed on the surface of many immune cells, such as activated monocytes, dendritic cells (DCs), natural killer (NK) cells, and T-cells, which plays a key role in regulating T-cell mediated responses: when PD-1 binds to PD-L1 on other cells, it sends an inhibitory signal that reduces the activity of the T-cell, essentially preventing it from attacking. This leads to a reduction of cytokines secretion, such as IL-2, IFN-γ, and tumor necrosis factor α (TNF-α), and cell proliferation by interfering with CD28-costimulatory signaling pathway. This mechanism is physiologically used by the immune system to maintain self-tolerance and preventing autoimmunity, limiting the excessive immune responses that can damage normal tissues. However, many tumors, including NSCLC, exploit this pathway by overexpressing PD-L1, and so deactivating T-cells and evading immune surveillance. This mechanism was used to develop immunotherapies, such as anti-PD-1 and anti-PD-L1 antibodies, which block this interaction and restore T-cell activity. Anti-PD-1/anti-PD-L1 has become the standard second-line therapy for patients whose disease progresses after platinum-based chemotherapy, and anti-PD-L1 agents such as Atezolizumab and Durvalumab have been approved for the patients with metastatic NSCLC[30]. Cytotoxic T lymphocyte antigen-4 (CTLA-4) is a competitive inhibitor

of CD28, a receptor that transduces co-stimulatory signals necessary for T cell activation and survival. CTLA-4 is often found overexpressed in cancer, suggesting a role in the suppression of the anti-tumor immune response[31]. Currently, anti-CTLA-4 antibody Ipilimumab in combination with Nivolumab (anti-PD-1) is approved for NSCLC patients with no EGFR or ALK mutations[32].

While naked-monoclonal antibodies target immune system checkpoints or block tumor antigens involved in cell growth, antibodies conjugated with different molecules are used to mediate specific delivery and bispecific antibodies can redirect immune cells to cancer cells. Another effort in this direction is being done by engineering of T- or NK cells to tumor antigens and reprogram the immune cells' behavior toward cancer cells, with most of these studies involving CAR-T cells. Despite this, T-cell therapy is not yet used in NSCLC due to difficulties in target choice, T-cell homing, and persistence.

Finally, cancer vaccines encourage immune response by showing tumor-associated-antigens, producing an adaptive anti-tumor response, although no vaccine for NSCLC has been approved yet and this approach is still under evaluation[28,29].

### 1.5 Drug resistance in NSCLC

Despite the initial response to therapies, tumors become resistant to treatments due to different reasons, including genetic mutations, epigenetic modifications, increased drug efflux, and various other cellular and molecular pathways. Overall, drug resistance arises because of tumor heterogeneity: solid tumors usually follow a branching evolution, hence a divergent propagation of multiple subclones of cancer cells that share the same ancestor, under the therapeutic selective pressure, which leads to a variety of responses to anticancer drugs[33]. Cancer cells ignoring cellular death signals, acquiring mutations, and bypassing signaling pathways can determine the onset of resistance.

Mechanisms of platinum-based chemotherapy resistance involve (I) reduced intracellular accumulation of platinum, mediated by increased efflux activity and decreased uptake, and mainly controlled by adenosine triphosphate (ATP) -binding cassette (ABC) transporters superfamily; (II) cancer stem cell differentiation in several cancer cell types under the stimulation of therapy; (III) a hypoxic TME leading to decreased apoptosis and increased survival pathways; (IV) mesenchymal-epithelial transition and autophagy; (V)

immunosuppressive microenvironment; (VI) reduced ROS accumulation in cancer cells through overexpression of glutathione or metallothioneins, known antioxidant factors; (VII) a wide activation of DNA repair mechanisms that avoid tumor cells death, downregulating proapoptotic proteins and promoting survival[34,35].

Activation of signaling downstream of EGFR, such as PI3K/AKT, MAPK, NF-kB, and JAK/STAT pathways, as well as upregulation of development pathways, like Notch or Wnt/β-catenin, also contributes to chemoresistant phenotypes. Radiotherapy resistance is linked to the dysregulation of these same pathways, as it can be induced by the increase of ROS accumulation, a consequence of radiotherapy itself, and it leads to enhanced antioxidant systems, increased double-strand-DNA breaks repair, upregulated survival, hypoxia and EMT pathways[35].

Resistance to targeted therapies generally arises when there is any modification to the target, such as secondary-tertiary kinase domain mutations on EGFR-mutated NSCLC or ALK-rearranged NSCLC, which prevents the link between TKIs and mutated oncogenes, or the amplification of an already mutated oncogene. One of the most frequent secondary mutations in the EGFR gene – present in 50% of patients with NSCLC who relapse after an initial response to TKIs – that confers acquired resistance to EGFR TKIs such as gefitinib and erlotinib is the T790M mutation in exon 20, which affects the catalytic domain of the kinase and results in a weaker interaction of the inhibitor with its target. Moreover, off-target mechanisms of resistance include loss of the tumor suppressor phosphatase and tensin homologue (PTEN), Insulin-like growth factor receptor 1 (IGFR1), ERBB3 or activated ERBB2 expression, as well as activating mutations of KRAS, HER2 amplification, RET rearrangement, or activation of bypass downstream signaling pathways, such as alternative receptor tyrosine-kinase (RTK) activation, of which the most common activated in EGFR-mutant NSCLC is the MET RTK, or direct downstream oncogene activation[35,36,37].

Finally, resistance to ICIs is due to a lack of recognition of tumor antigens from T-cells, caused by the absence of the antigens or changes in their presentation mechanisms, and by the onset of tumor evasion strategies[28]. Immunoresistence relies on genetic alterations modifying the expression of ICPs, enhancing cancer cell proliferation and metastasis by the upregulation of PI3K/AKT, IFNγ/JAK/STAT, and Wnt/β-catenin signaling. Moreover, the angiogenic pathways and immunosuppressive microenvironment can inhibit the immune-infiltrations into TME, reducing adhesion molecules, releasing pro-inflammatory molecules, and upregulating

ICPs and their alternative forms. Another cause of immunoresistance is T-cell exhaustion due to chronic exposition to antigens[28,38].

Paracrine signaling plays a significant role in driving drug resistance in NSCLC by promoting an immunosuppressive tumor microenvironment (TME), supporting cancer cell survival and evasion of immune response. Tumor cells and surrounding stromal cells release cytokines and growth factors, such as VEGF, IL-6 and TGF-β, which promote survival pathways in cancer cells and support immune evasion. The production of immunosuppressive cytokines, which include chemokines, growth factors, pro and antiangiogenic factors, adipokines, soluble receptors and extracellular proteases, is an extensively studied aspect of resistance drug resistance. These factors guide processes such as epithelial-mesenchymal transition (EMT), autophagy, and resistance to apoptosis, enabling cancer cells to evade the cytotoxic effects of chemotherapy, immunotherapy, and targeted therapies. Cytokines recruit and activate tumor-associated macrophages and myeloid-derived suppressor cells, which produce additional immunosuppressive factors that reduce immune cell infiltration and activity within the TME, further protecting cancer cells from immune checkpoint inhibitors, and they are able to induce the expression of transporters, such as P-glycoprotein, that extrude chemotherapeutics, and so protecting cancer cells from chemotherapy-induced apoptosis. Moreover, these factors are able to activate signaling pathways, including NF-κB, PI3K/AKT, JAK/STAT, and MAPK pathways, that enhance cancer cells survival, proliferation and resistance to apoptosis[39,40,41].

Another source of paracrine signals that gained a large interest in the last few years is represented by extracellular vesicles (EVs). EVs are a group of nano-sized particles incapsulated by a lipid bilayer that can be actively released by any cell. EVs exert most of the functions of their parental cell, as they carry signals that promote survival, proliferation, and metastatic potential in recipient cancer cells, and so enhancing resistance to therapies. It is known that treatments increase the production of EVs from NSCLC cells, mostly of which carry immunomodulatory functions. For example, EVs can present antigens to T-cells, acting as primary effectors of T-cells activation or inhibiting the immune cells functions, or they can expose PD-L1 on their surface to suppress the function of CD8 T-cells and evade immune-killing[42,43]. Moreover, recent studies highlighted how cancer cells use EVs to transfer oncogenic ALK to healthy cells in the TME and confer resistance to drug-sensitive cancer cells, via activation of the MAPK pathway, and that EVs carry oncogenic micro RNAs (miRNAs) and

long non coding RNAs (lncRNAs) associated with therapy resistance: it is the case of EVs that transport miR-214, the lncRNA H19, and the miR-21, associated with gefitinib resistance, or EVs that transport miR-182, associated with cisplatin resistance[43,44,45].

In this context, targeting paracrine interactions in the TME is emerging as a strategy to overcome resistance in NSCLC and enhance treatment efficacy.

### 1.6 The role of JAK/STAT pathway in drug resistance

The JAK-STAT signaling pathway is universally expressed in response to cytokines, and growth factors signals, and it is involved in many biological processes and immune functions. Following IFNγ binding to its membrane receptor, which dimerizes, JAK kinase phosphorylates the receptor's intracellular tyrosine-residues to recruit STAT proteins and cause their phosphorylation and dimerization. Dimerized STATs migrate toward the nucleus, where they regulate the cytokines-responsive gene expression by binding specific DNA elements. JAK kinases are also activators of PI3K/AKT/mTOR signaling involved in survival and proliferation. Hyperactivation of JAK-STAT signaling is associated with different tumors, including lung cancer, and it is being studied as a novel therapeutic target[46]. JAK mutations cause the blockade of IFNγ-signaling, promoting immuno-evasion and insensitivity to PD-1/PD-L1 immunotherapy. Inhibitors of STAT proteins have shown re-sensitization of resistant NSCLC to cisplatin.

STAT1 is an essential component of IFN-signaling and it has a controversial role as a tumor-promoting or suppressor factor. As a downstream mediator of IFNγ, STAT1 can promote cell-cycle arrest and apoptosis, inducing proapoptotic genes, and expression of p53, facilitating chemotherapy-induced cell death. It can inhibit proangiogenic factors and angiogenesis, and negatively regulate metastasis. IFNγ-STAT1 signaling promotes antigen presentation through MHC, enhancing immunosurveillance. In different types of tumors, it was found that aberrant STAT1 expression correlates with tumorigenesis. Indeed, STAT1 can downregulate its negative regulators (such as SOCS1 and PIAS1), it can increase proliferation, survival, and antiapoptotic gene expression. STAT1 can also induce pro-inflammatory cytokine production, promoting chronic inflammation which favors tumorigenesis. STAT1's dual role is determined by the tumor type and microenvironment, and it's still not entirely clear in lung cancer[47,48].

Although IFNγ is upregulated in immune cells in response to immunotherapy, allowing cytostatic effect on tumor cells, it can also support tumor growth increasing PD-L1 expression in cancer and realizing adaptive resistance via the activation of JAK/STAT1 and PI3K/AKT pathways. PI3K/AKT pathway is involved in IFNγ-mediated activation of STAT, which is essential in enhancing PD-L1 expression. Therefore, a potential therapeutic approach may be represented by a combination of PI3K inhibitor plus IFNγ, causing an antiproliferative effect and decreased immune escape due to a reduced PD-L1 expression[49,50]. The response to anti-PD-1/anti-PD-L1-based immunotherapy depends on the expression of immune checkpoints, with a favorable outcome in patients with tumors expressing PD-L1>1%[51].

## 2. Aim of the study

Despite new therapeutic strategies that improved the prognosis of NSCLC patients and their quality of life, lung cancer tends to reoccur, because of therapy resistance and immune-evasion. At the basis of these events is the dysregulation of signaling pathways involved in survival and proliferation, and the JAK/STAT pathway is one such example. This work aims to investigate the molecular mechanisms of therapy resistance in NSCLC, focusing on JAK/STAT signaling as a crucial pathway at the basis of resistance to chemotherapy and immune-killing, and specifically on the controversial role of STAT1 in lung cancer.

Starting from the preliminary data on JAK/STAT axis as mediator of chemoresistance and tumor-induced immune-suppression, the first part of this thesis focused on exploring how JAK/STAT pathway acts in the resistance to chemotherapy and the immune system action. STAT1 was found to mediate NSCLC cells' resistance to cisplatin and paclitaxel-based chemotherapy and immune-killing by T-lymphocytes, with paracrine mechanisms involved in the process.

In a second part of this thesis, the resistance to EGFR inhibitors was addressed, using erlotinib-sensitive and erlotinib-resistant NSCLC cells. A panel of top-compounds that are significantly more effective than erlotinib were identified, independently from classical mechanisms of resistance to EGFR inhibitors, such as mutations in EGFR gene itself.

Overall, this work explored the most crucial aspects of therapy resistance in NSCLC, identified a role for the JAK/STAT pathway in chemo-immuno-resistance and a potential therapeutic approach to counteract EGFR inhibitors resistance.

## 3. Materials and methods

### 3.1 Chemicals

Plasticware for cell culture was purchased from Falcon (Becton Dickinson, Franklin Lakes, NJ, USA). Culture medium, and fetal bovine serum (FBS) from Sigma Aldrich (St. Louis, MO, USA). The protein content was assessed with BCA kit (Sigma-Merck, St. Louis, MO, USA). Cisplatin (cis-diammineplatinum(II) dichloride, cat # P4394) and Paclitaxel (cat# T7191) were purchased from Sigma-Merck. Electrophoresis reagents were from Bio-Rad Laboratories (Hercules, CA, USA). If not specified, other reagents were from Sigma-Merck.

### 3.2 Cells

Human NSCLC cells (A549, Calu-3, NCI-H1395, NCI-H1650, NCI-H1975, NCI- H2228) and non-malignant human bronchial epithelial lung Beas-2B cells were purchased from ATCC (Manassas, VA, USA). Cells were grown in RPMI 1640 medium, except for A549 cell line which was grown in DMEM medium, supplemented with 100 µL/mL FBS, 100 U/mL penicillin and 0,1 mg/mL streptomycin, into Heracell incubator.

### 3.3 Cell viability

#### 3.3.1 WST-1 assay

WST-1 reagent was purchased from Roche (Roche Diagnostics GmbH, Mannheim, Germany). Briefly, cells were seeded in a 96-well plate, 5.000 cells/well, and were then exposed to different concentrations of either 50 µM cisplatin, 25 nM paclitaxel, a combination of these two drugs or different concentrations of other test compounds, namely 1 nM, 10 nM, 100 nM, 1 µM, 5 µM, 10 µM, 25 µM, 50 µM, 100 µM, 250 µM and 500 µM of erlotinib or compound 2–6, alone or in the presence of 50 µM N-acetylcysteine (NAC). After the 72h transfection time, cell proliferation and viability reagent WST-1 (Sigma Aldrich) was added 1:10 to the medium for each well. Plates were incubated at 37°C, 5% CO2, for a total of 4 hours. Synergy HT Multi-Detection Microplate Reader (Bio- Tek Instruments, Winooski, VT, USA) was used to measure the absorption at 440nm and at 636nm as reference wavelength, every 30 minutes. The absorbance of control NSCLC cells was considered as 100% viability; the results were expressed as a percentage of treated cells versus control cells.

### 3.3.2 Crystal violet assay

NSCLC cells were stained with 5% v/v crystal violet solution in 20% v/v methanol for 30 min, washed, dried and photographed. Quantitation of crystal violet staining was performed after solubilizing the dye with 10% v/v acetic acid. Then, the plates were analyzed with Synergy HT Multi-Detection Microplate Reader (Bio-Tek Instruments, Winooski, VT, USA), using Gene5 Software, to measure the absorbance at 540 nm. The absorbance of control NSCLC cells was considered as 100% viability; the results were expressed as a percentage of treated cells versus control cells.

### 3.4 Annexin V assay

Cells were grown for 48 h in a fresh medium (Ctrl) or in medium containing 20 μM of Erlotinib compound 3. Then they were detached and washed twice with fresh phosphate buffered saline (PBS) solution and apoptosis assay was performed using Annexin-V-FLUOS Staining Kit (Roche) according to manufacturer's instruction. For each analysis, 10.000 events and were collected and samples were analyzed with a FACS-Calibur flow cytometer (Becton Dickinson). The results were expressed as % of positive cells, calculated with the Cell Quest software (Becton Dickinson).

### 3.5 Caspase-3 and -9 activation assay

Cells were grown for 48 h in a fresh medium or in medium containing 20 μM of Erlotinib compound 3. Then cells were lysed in 0.5 mL of caspase lysis buffer (20 mM Hepes/KOH, 10 mM KCl, 1.5 mM $MgCl_2$, 1 mM EGTA, 1 mM EDTA1, 1 mM DTT, 1 mM PMSF, and 10 μg/mL leupeptin, pH 7.5). The 20 μg of cell lysates were incubated for 1 h at 37 ◦C with 20 μmol/L of the fluorescent substrate of caspase-9 Ac-Leu- Glu-His-Asp-7-amino-4-methylcoumarin (LEHD-AMC) or of caspase-3 Ac-Asp-Glu-Val-Asp-7-amino-4-methylcoumarin (DEVD-AMC), in 0.25 mL of caspase assay buffer (25 mM Hepes, 0.1% w/v 3-[(3-cholamido- propyl)dimethylammonio]-1-propanesulfonate (CHAPS), 10% w/v sucrose, 10 mM DTT, 0.01% w/v egg albumin, pH 7.5). The reaction was stopped by adding 0.75 mL of ice-cold PBS 0.1% w/v trichloroacetic acid. The fluorescence of each sample was read using a Synergy HT Multi- Mode Microplate Reader (BioTek) at 488 nm (λ excitation) and 520 nm (λ emission). Fluorescence was converted in nmol/mg cell proteins, using a calibration curve prepared previously with standard solutions of AMC.

### 3.6 Cell cycle analysis

Cells were grown for 48 h in a fresh medium or in medium containing 20 μM of Erlotinib compound 3. Then cells were detached and washed twice with fresh PBS, incubated in 0.5 mL ice-cold ethanol 70% v/v for 15 min, then centrifuged at 13,000 rpm for 5 min at 4 °C and rinsed with 0.3 mL of citrate buffer (50 mM $Na_2HPO_4$, 25 mM sodium citrate, 1% v/ v Triton X-100), containing 1 μg/mL propidium iodide and 1 μg/mL ribonuclease (RNase). After 15 min incubation in the dark, the intracellular fluorescence was detected by flow cytometry. For each analysis, 20.000 events were collected and the cell-cycle distribution G0/G1, S, and G2/M was analyzed by Guava®easyCyte flow cytometer (Millipore, Billerica, MA, USA), equipped with the InCyte software (Millipore).

### 3.7 Changes in mitochondrial transmembrane potential

Cells were grown for 48 h in a fresh medium or in medium containing 20 μM of Erlotinib or compound 3. Cells were detached, washed twice with fresh PBS, and $1\times10^6$ cells were re-suspended in 0.5 mL PBS. Then they were incubated for 30 min at 37 °C with 2 μmol/L of the fluorescent probe JC-1 (Biotium Inc., Hayward, CA), centrifuged at 13,000 × g for 5 min and resuspended in 0.5 mL PBS. The fluorescence of each sample was read using a Synergy HT Multi-Mode Microplate Reader (BioTek): the red fluorescence, index of polarized mitochondria, was read at 550 nm (λ excitation) and 600 nm (λ emission); the green fluorescence, index of depolarized and damaged mitochondria, was detected at 485 nm (λ excitation) and 535 nm (λ emission). The fluorescence units were used to calculate the percentage of green fluorescent versus red-fluorescent mitochondria.

### 3.8 Cytokines array

Cytokine array experiment was performed using the Human Cytokine Antibody Array (cat. #ab133998, Abcam, Cambridge, UK). Membranes were incubated with 2 mL of blocking buffer each, for 30 min at room temperature, on a rocking platform. After blocking buffer removal, membranes were incubated overnight with 1 mL of sample (medium from $1x10^6$ cells from a 100 mm Petri dish). After washing, each membrane was incubated, for 90 min on a rocking platform, with the primary biotinylated antibody. Membranes were then incubated with streptavidin for 2 h in agitation. After an additional washing, detection buffer (provided by the

kit) was used to detect the chemiluminescence with ChemiDoc™ Touch Imaging System device (Bio-Rad Laboratories).

### 3.9 DNA damage assay

NCI-H1975 and NCI-H1650 cells were seeded overnight onto glass coverslips and then cells were grown for 48 h in a fresh medium or in medium containing 20 μM of Erlotinib compound 3. Cells were washed with PBS and fixed using 4% w/v paraformaldehyde for 15 min at room temperature, permeabilizated with 0.1% v/v Triton X-100 in PBS and then washed 3x with PBS. Samples were incubated over night at 4 °C with anti-gamma H2AX antibody (Abcam; diluted 1:100 in 1% FBS/PBS). PBS was used to wash the samples five times; samples were then incubated for 1 h at room temperature with an Alexa Fluor® 553-conjugated secondary antibody (diluted 1:100 in 1% FBS/PBS; Abcam). Then the cells were mounted with DAPI mount (Sigma). The samples were examined with a Leica DC100 fluorescence microscope, ocular 10x, objective 100x.

### 3.10 ELISA assay

ELISA assay was performed according to the manufacturer's instructions. Total amount of GRO-α was quantified in NSCLC cells' medium from 0,5 x $10^6$ cells using Human GRO-α/MGSA (CXCL1) Standard ABTS ELISA Development Kit (cat n. 900-K38; PeproTech, Cranbury, New Jersey, USA). ABTS (2,2′-Azino-bis-3-ethylbenzothiazoline-6-sulfonic acid; cat. N. A3219, Sigma-Merck, St. Louis, MO, USA) was used as substrate solution for the assay. Results were expressed in μg/mL.

### 3.11 Extracellular Vesicles isolation and characterization

EVs were isolated from NCI-H2228 cell line media by using the differential centrifugation method reported in[52]. "10 k EVs pellet" indicates EVs obtained after 10.000 g centrifugation. Instead, EVs isolated after 100.000 g centrifugation were referred to as "100 k EVs pellet". According to the International Society of Extracellular Vesicles (ISEV), the characterization of different EV populations was performed using the following diverse methods:

#### 3.11.1 Nanoparticle Tracking Analysis (NTA)

To measure the Brownian movement rate of particles a NanoSight NS300 system (Malvern Instruments, U.K), equipped with fast video capture and particle-tracking software, was used.

Mean, mode, median vesicle size (nm), and estimation of particle concentration (particle/mL) were evaluated.

### 3.11.2 Transmission electron microscopy (TEM)

Each sample was deposited onto Formvar-carbon coated electron microscopy grids for 1-2 min in the dark at room temperature. EVs were stained with 1% uranyl acetate and visualized under the TEM (Joel, JEM 1400) with an acceleration voltage of 80kV. Then digital images of EVs were obtained.

### 3.11.3 Immunoblotting

15 µg of proteins from the 100 k EVs pellet (quantified using a modified version of the Lowry assay; DC Protein Assay, Bio-Rad) or 2.96 x $10^7$ particles from the 100 k EVs pellet (quantified by NTA) were separated by SDS-PAGE. Specific EV markers were probed with the following antibodies: anti-TSG101 (sc136111, Santa Cruz Biotechnology), anti-Alix (sc49268, Santa Cruz Biotechnology), anti-Actinin-4 (sc390205, Santa Cruz Biotechnology), anti-Annexin XI (sc46686, Santa Cruz Biotechnology), anti-Cytochrome C (sc13560, Santa Cruz Biotechnology), anti-GAPDH (sc47724, Santa Cruz Biotechnology).

### 3.11.4 Proteomics analysis

The proteins were solubilized with 100 mM Tris pH 8.5, 1% sodium deoxycholate, 10 mM tris(2-carboxyethyl) phosphine (TCEP), 40 mM chloroacetamide and protease inhibitors, and mixed for 10 min at 95 °C at 1000 rpm (Thermomixer, Eppendorf). The solid-phase-enhanced sample-preparation protocol was used to process each sample for proteomics analysis. Trypsin/LysC (2µg)-based enzymatic digestion was performed overnight, incubated at 1000rpm at 37 °C. Nano LC-MS/MS was used for protein identification and quantitation. The equipment includes Ultimate 3000 liquid chromatography system coupled to a Q-Exactive Hybrid Quadrupole-Orbitrap mass spectrometer (Thermofisher Scientific, Bremen, Germany). Samples were loaded onto a trapping cartridge in a mobile phase of 2% ACN, 0,1% FA at 10 µL/min. After 3 min loading, the trap column was switched in-line to a 50 cm by 75 µm inner diameter EASY-Spray column at 300 nL/min. Separation was generated by mixing 0,1% FA (A) and 80% ACN (B) with the following gradient: 5 min (2.5% B to 10% B), 120 min (10 % B to 30 % B), 20 min (30% B to 50% B), 5 min (50% B to 99% B) and 10 min (hold 99% B). Then, the column was equilibrated with 2,5% B for 17 min. Acquired data were controlled by

Xcalibur 4.0 and Tune 2.9 software (Thermo Scientific, Bremen, Germany). The mass spectrometer was operated in data-dependent (dd) positive acquisition mode alternating between a full scan (m/z 380-1580) and subsequent HCD MS/MS of the 10 most intense peaks from full scan (normalized collision energy of 27%). ESI spray voltage was 1.9 kV. Global settings: use lock masses best (m/z 445.12003), lock mass injection Full MS, peak width (FWHM) 15s. Full scan settings: 70 k resolution (m/z 200), AGC target 3e6, maximum injection time 120 ms. dd settings: minimum AGC target 8e3, intensity threshold 7.34, charge exclusion: unassigned, 1, 8, >8, peptide match preferred, exclude isotopes on, dynamic exclusion 45s. MS2 settings: microscans 1, resolution 35k (m/z 200), AGC target 2e5, maximum injection time 110 ms, isolation window 2.0 m/z, isolation offset 0.0 m/z, spectrum data type profile. The raw data was processed using the Proteome Discoverer 2.3.0.523 software (Thermo Scientific) and searched against the UniProt database (2019_04) for the Homo sapiens proteome, and a common contaminant database. To identify tryptic peptides was uses Sequest HT search engine. The ion mass tolerance was 10 ppm for precursor ions and 0.02 Da for fragmented ions. 2 is the maximum allowed missing cleavage sites. Cysteine carbamidomethylation was defined as a constant modification. Methionine oxidation and protein N-terminus acetylation were defined as variable modifications. Peptide confidence was set to high. The processing node percolator was enabled with the following settings: maximum delta Cn 0.05; decoy database search target FDR 1%, validation based on q-value. Protein label-free quantification was performed with the Minora feature detector node at the processing step. Precursor ions quantification was performed at the processing step with the following parameters: peptides to use unique plus razor, precursor abundance was based on intensity, normalization mode was based on total peptide amount, pairwise protein ratio calculation, hypothesis test was based on t-test (background based).

### 3.12 Gene Silencing

2 x $10^5$ cells were seeded in 6 well plates and grown until 60-80% of confluency. Then, cells were transfected with 2 μg of plasmid encoding for a short-hairpin RNA targeting STAT1 gene (abx954629; Abbexa, Cambridge, UK) or a negative control plasmid (abx991273; Abbexa, Cambridge, UK), using jetPRIME transfection reagent (Cat. #101000046, Polyplus, New York, NY, USA). The efficacy of silencing was assessed by immunoblotting (24h, 48h, 72h, 96h after the transfection). When unspecified, transfected cells were collected at the 72 h timepoint.

### 3.13 Immunoblotting

Cells were lysed in RIPA Lysis buffer (50 mM Tris, pH 7.4, 250 mM NaCl, 5 mM EDTA, 50 mM NaF, 1 mM $Na_3VO_4$, 1% NP-40, 0.02% $NaN_3$) with protease inhibitor cocktail set III (Sigma Aldrich, cat # P8340) in a ratio of 1:100. They were sonicated (2 cycles of 10s for each sample, 4°C, 40 Hz, Labsonic sonicator, Hielscher, Teltow) and centrifuged at 13000 rpm for 5 min at 4°C. 15 µg of proteins were subject to immunoblotting (4-20% gradient SDS-page and semi-dry transfer on PVDF membranes from Bio-Rad Laboratories) and probed with the following antibodies: anti-GAPDH (sc-47724, Santa-Cruz Biotechnology) used as a control of equal protein loading, anti-STAT1 (#14994, Cell Signaling, Danvers, MA, US), anti-pSTAT1 (#9167, Cell Signaling), anti-PD-L1 (sc293425, Santa Cruz Biotechnology), anti-histone H3 (ab1791, Abcam), used as equal protein loading control for nuclear protein extracts. After washing in TBS (Tris- buffer saline solution, pH 7.4) with 1% v/v Tween, proteins were stained with a peroxidase-conjugated secondary antibody and were detected by enhanced chemiluminescence (Bio-Rad Laboratories) with a ChemiDoc™ Touch Imaging System device (Bio-Rad Laboratories). The relative quantitation of immunoblot was performed with the ImageJ software.

### 3.14 Lymphocytes proliferation assay

Blood samples were obtained from healthy blood donors (Blood Bank of the AOU Città della Salute e della Scienza, Torino, Italy; DG 767/2015). After isolation on the Ficoll-Hypaque density gradient, peripheral blood mononuclear cells (PBMCs) were stained using BioTracker 488 Green CSFE Cell Proliferation Kit (Sigma- Merck, SCT110). PBMCs were seeded $0.5x10^6$ cells/well, or 1:10 to NSCLC cells. T-cells activation was induced with the addition of IL-2 (Abnova, cat# P5822), CD3 Monoclonal Antibody (Invitrogen, Cat #16-0037-81) and CD28 Monoclonal Antibody (Cat #16- 0289-85). PBMCs were cultured for 72h with NSCLC cell lines, and were then collected from co-cultures and centrifuged at 1700rpm for 5 min. Supernatant was discarded, cells were washed with 500 µL of PBS pH 7.4, and centrifuged again at 1700 rpm for 5 min. Supernatant was discarded and cells were resuspended with 300 µL of PBS. Proliferating cells were analyzed by flow cytometry using the BD Accuri™ C6 flow cytometer (BD Biosciences, Franklin Lakes, New Jersey, U.S.), equipped with the Accuri™ C6 software (BD Biosciences, Franklin Lakes, New Jersey, U.S.).

### 3.15 Lymphocytes activation assay

Blood samples were obtained from healthy blood donors (Blood Bank of the AOU Città della Salute e della Scienza, Torino, Italy; DG 767/2015). After isolation on the Ficoll-Hypaque density gradient, PBMCs were cultured for 72h with NSCLC cell lines in a 1:10 ratio (5 x $10^4$ NSCLC cells with 5 x $10^5$ PBMCs in a 24 well plate) and incubated for 4 h with CD107a (LAMP-1) Antibody (anti-human, PE, REAfinity™; cat. 130-111-621, Miltenyi Biotec, Bergisch Gladbach, North Rhine-Westphalia, Germany), a T-cell activation indicator, and CD3 Antibody (anti-human, PerCP-Vio® 700, REAfinity™, Miltenyi), a T-cell marker. Activation was assessed in flow cytometry. Results were expressed as percentage of proliferating cells incubated with STAT1-silenced NSCLC cells vs control.

### 3.16 Nuclear extracts

Nuclear extraction was performed using the Nuclear Extract Kit (cat. #40010, 40410; Active Motif). After 72h of transfection cells were resuspended in 500µL 1X Hypotonic Buffer and incubated for 15min on ice. Samples were supplemented with 25µL of detergent and vortexed 10 sec. Suspensions were centrifuged for 30 sec at 14,000 rpm in a microcentrifuge pre-cooled at 4°C. The supernatants obtained were the cytoplasmatic fraction. The pellets obtained were used for nuclear fraction collection. Nuclear pellets were resuspended in 50 µL of Complete Lysis Buffer and then vortexed for 10 sec. Suspensions were incubated for 30 min on ice on a rocking platform set at 150 rpm. Samples were vortexed for 10 sec and then centrifuged for 10 min at 14000 rpm in a microcentrifuge pre-cooled at 4°C. The supernatants obtained are the nuclear fraction. Nuclear fractions were quantified with Bradford assay (Cat. #5000205, Bio-Rad Laboratories), and results were read with Synergy HT Multi-Detection Microplate Reader (Bio-Tek Instruments, Winooski, VT, USA).

### 3.17 PCR array

Total RNA was extracted by using TRItidy G (VWR International), and reverse transcription was performed by using iScript™ cDNA Synthesis Kit (Bio-Rad Laboratories). PCR arrays were conducted by using iTaq™ Universal SYBR® Green Supermix (Bio-Rad Laboratories) and performed on 1µg cDNA, using customized PrimePCR™ Arrays pre-coated with primers for innate and adaptive immune response genes (Bio-Rad Laboratories, cat #10034180). The

quantification was performed using the Bio-Rad Software Gene Expression Quantitation (Bio-Rad Laboratories).

### 3.18 Reactive oxygen species (ROS) generation

Cells were grown for 1h in a fresh medium or in medium containing 20 μM of Erlotinib compounds 2–6, with or without 50 μM NAC. Then cells were detached from dishes and re-suspended in 0.5 mL PBS, incubated for 15 min at 37 °C with 10 μM of the fluorescent probe 5-(and-6)-chloromethyl-2',7'-dichlorodihydrofluorescein-diacetate-acetyl-ester (CM-H2DCFDA), centrifuged at 13,000 rpm at 37 °C for 30 s and resuspended in 0.5 mL PBS. The fluorescence of each sample, considered an index of ROS levels, was read at 488 nm (λ excitation) and 520 nm (λ emission). The results were expressed as relative DCF fluorescence/mg cell proteins versus ctrl.

### 3.19 Statistical Analysis

Results were analyzed by a one-way analysis of variance (ANOVA) and Tukey's test, using GraphPad Prism software (v9.5.1, San Diego, CA, USA). $p < 0.05$ was considered significant. All data were expressed as means ± SD.

## 4. Results

### 4.1 STAT1 is highly expressed in NSCLC cells but its silencing does not alter PD-L1 expression

In order to evaluate the involvement of leading pathways of resistance in NSCLC, the different innate and adaptive immune response factor genes were screened in six different NSCLC cell lines showed high expression of STAT1 (**Figure 1A**), additionally confirmed at the protein level (**Figure 1B**). Based on basal expression of STAT1 and PD-L1, two NSCLC cell lines, Calu-3 and H2228, were selected for further experiments. STAT1-silencing was effectively standardized and evaluated at different time points as total protein extract or nuclear protein extract (**Figure 1C**; **Figure 1D**), although it did not show any effect on PD-L1, which was examined as both an immune-resistance indicator and a factor regulated by the JAK/STAT1 pathway[53].

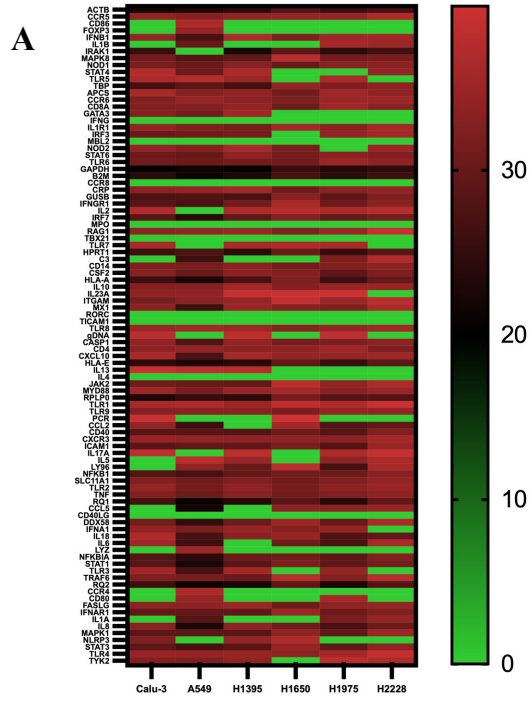
A
Calu-3
A549
H1395
H1650
H1975
H2228
30
20
10
0

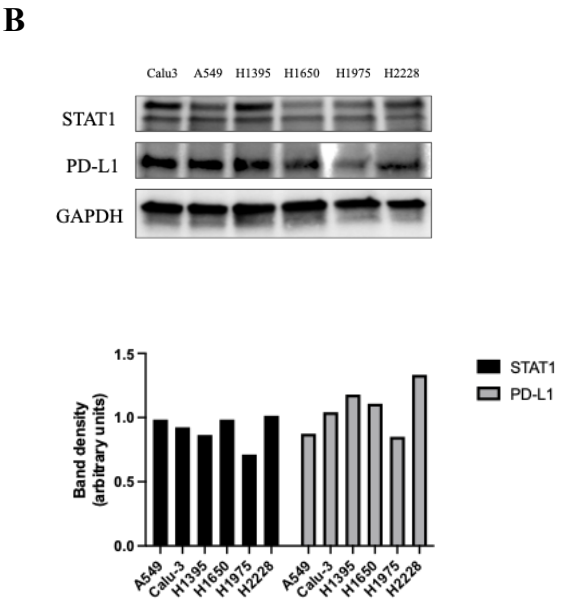
B
Calu3
A549
H1395
H1650
H1975
H2228
STAT1
PD-L1
GAPDH
Band density (arbitrary units)
1.5
1.0
0.5
0.0
STAT1
PD-L1
A549
Calu-3
H1395
H1650
H1975
H2228

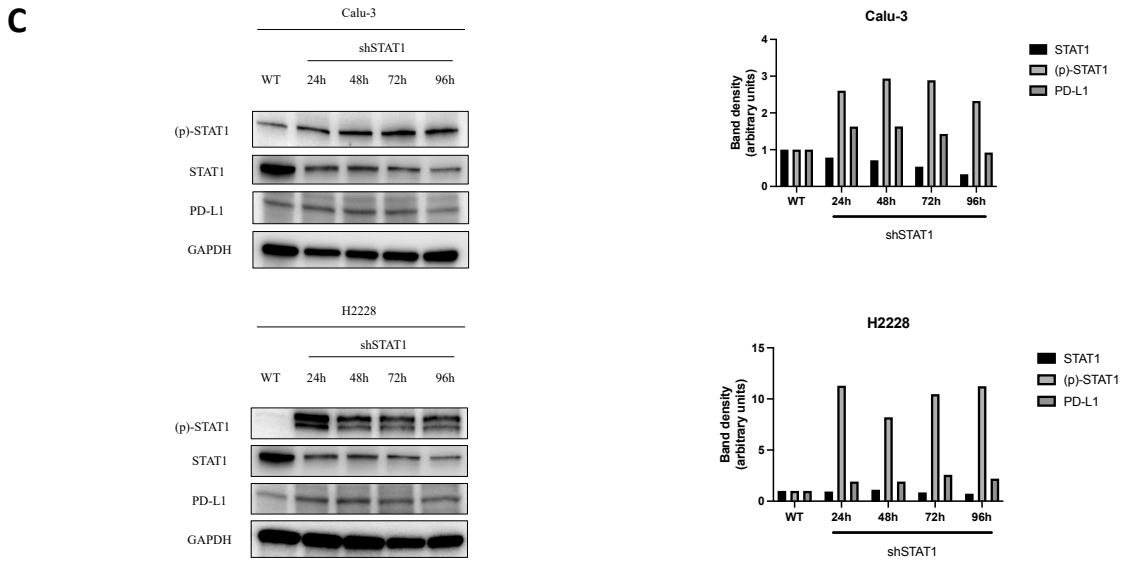
C
Calu-3
shSTAT1
WT
24h
48h
72h
96h
(p)-STAT1
STAT1
PD-L1
GAPDH
H2228
shSTAT1
WT
24h
48h
72h
96h
(p)-STAT1
STAT1
PD-L1
GAPDH
Calu-3
Band density (arbitrary units)
STAT1
(p)-STAT1
PD-L1
WT
24h
48h
72h
96h
shSTAT1
H2228
Band density (arbitrary units)
STAT1
(p)-STAT1
PD-L1
WT
24h
48h
72h
96h
shSTAT1

**D**

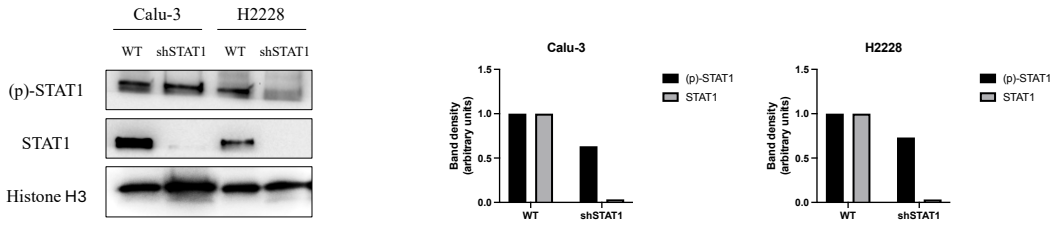


***Figure 1.*** STAT1 is highly expressed in NSCLC cells, both at RNA and protein levels. **A)** Heatmap of innate and adaptive immune response genes, including STAT1 and other members of the STAT family, obtained by screening six commercial NSCLC cell lines via PCR array (n=3). **B)** Immunoblot of indicated proteins in NSCLC cell lines and immunoblot quantitation. The quantitation of the band density was performed using the ImageJ software. GAPDH was used as control of equal protein loading. Pictures are representative of one out of two independent experiments. **C**) Immunoblot of Calu-3 and H2228 cell lines, both wild-type (WT) and silenced for STAT1 gene (shSTAT1), and collected respectively at 24h, 48h, 72h, and 96h, and immunoblot quantitations. Results show effective STAT1 silencing at all timepoints, but no variation in PD-L1 and phosphorylated pSTAT1 expression. GAPDH was used as a control of equal protein loading. **D**) Immunoblot of nuclear extracts, from wild-type (WT) and STAT1-silenced (shSTAT1) Calu-3 and H2228 cell lines, further confirming STAT1 silencing at nuclear level, and immunoblot quantitations. Histone H3 was used as an equal protein loading control.

### 4.2 STAT1 silencing increases T-cell activation and immune-killing of NSCLC cells

Considered that previous experiments did not show any alteration in PD-L1 expression in STAT1-silenced cells but JAK/STAT pathway's role in immune resistance is widely acknowledged in literature[53], an analysis of STAT1's function in this setting was performed. Wild-type (WT) and STAT1-silenced (shSTAT1) NSCLC cells were co-cultured with PBMCs and then T-cells were analyzed. Results showed that silencing of STAT1 in H2228 cell line was able to increase the proliferation of co-cultured T-cells, indicating the possibility of re-sensitization to immune-killing in STAT1-silenced cells, while the same result was not observed in T-cells co-cultured with STAT1-silenced Calu-3 cells and H1395 cells (**Figure 2A**). Nevertheless, all cell lines showed a reduction of tumor cells viability (**Figure 2B**), suggesting an effective immune-killing from T-cells even in the absence of T-cell proliferation. Moreover, the expression of CD107, a marker of T-cell activation[54], was respectively 100% and 50% higher in T-cells co-cultured with STAT1-silenced Calu-3 cells and H2228 and H1395 cells compared to T-cells co-cultured with WT NSCLC cells (**Figure 2C**). Overall, these results suggest a role for STAT1 in immune-resistance, which may act by suppress T-cells activation and proliferation.

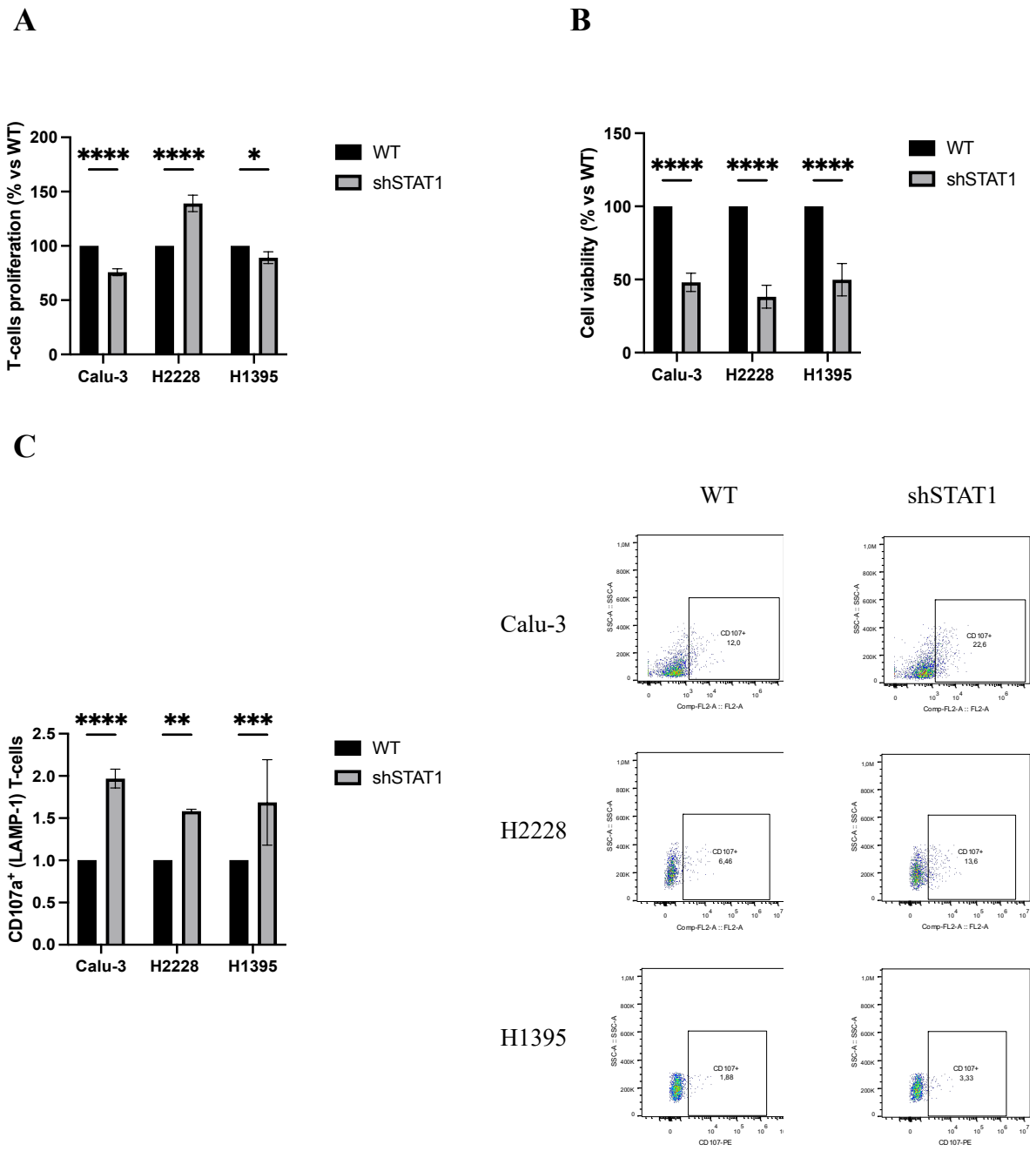


***Figure 2***. Silencing of STAT1 increases T-cell activation and immune-killing. (A) CFSE-based T-cell proliferation assay shows an increase of T-cell proliferation when they are co-cultured with STAT1-silenced H2228 cells. (B) T-cell immune-killing effects on NSCLC cells viability, measured spectrophotometrically after a crystal-violet staining. (C) Expression of CD107-positive cells, measured in flow cytometry, where CD107 was considered as a T-cells activation marker, and representative images of the cytofluorimetric acquisition. Data are expressed as means ± SD (n=2). * $p<0.05$, ** $p<0.005$, *** $p<0.0005$, **** $p<0.0001$.

### 4.3 STAT1 silencing increases chemosensitivity of NSCLC cells by releasing soluble factors in cell media

To evaluate the role of STAT1 in chemoresistance, STAT1-silenced NSCLC cells were treated with 50 μM cisplatin, 25 nM paclitaxel, or a combination of the two drugs, commonly used as front-line NSCLC treatment[55]. Compared to wild-type cells, STAT1-silenced Calu-3 (**Figure 3A**) and H2228 (**Figure 3B**) cells showed a remarkable viability reduction when treated with both drugs and their combination, although H1395 did not show the same tendency (**Figure 3C**). Moreover, given the fact that PD-L1 was found unmoved by STAT1 silencing despite an increase of T-cells activity towards silenced cells, to assess if these results were dependent on soluble factors present in the cell media, WT cells were cultured with medium coming from shSTAT1 cells and shSTAT1 cells were cultured with medium coming from WT cells for 72h. Results show that the chemosensitivity trend was reversed: the media exchange between the two conditions increased chemosensitivity of WT cells cultured in STAT1-silenced cells media and decreased chemosensitivity in STAT1-silenced cells cultured in WT cells media. These suggest not only that STAT1 is involved in chemoresistance and its silencing increases NSCLC cells' sensitivity to cisplatin and paclitaxel, but also that its mechanism of action may rely on soluble factors released in cell media.

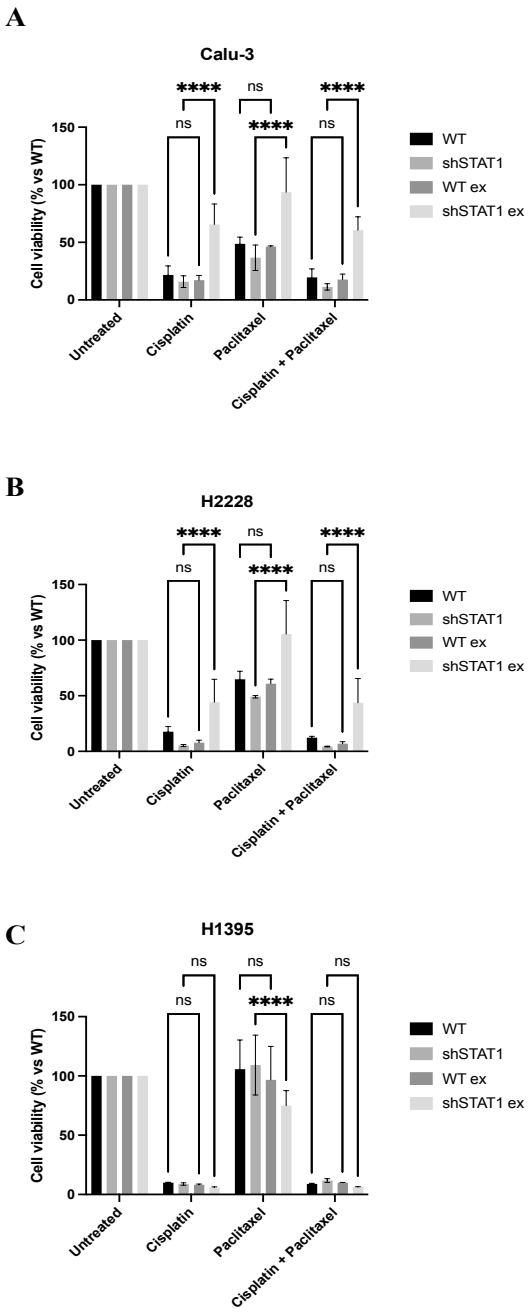


***Figure 3***. STAT1-silenced NSCLC cells show increased chemosensitivity. Cell viability, measured spectrophotometrically after WST-1 assay, of: WT, shSTAT1, WT with exchanged media (WT ex) and STAT1-silenced with exchanged media (shSTAT1 ex) Calu-3 (A), H2228 (B) and H1395 (C) cells treated with 50 μM cisplatin, 25 nM paclitaxel, or a combination of the two drugs for 72h. Data are expressed as means ± SD (n=3). Ns is non-significant, **** $p<0.0001$.

### 4.4 The potential role of paracrine signals: cytokines and extracellular vesicles

Given the involvement of STAT1 in chemo-immuno-resistance and its action through soluble factors, the differential production of such factors was assessed. First, the release of cytokines in WT vs STAT1-silenced NSCLC cells was investigated, and in all cell lines a downregulation of Groα and IL-8 was observed; moreover, in STAT1-silenced Calu-3 and H2228 cell line also MCP-1, Angiogenin, and TIMP2 expression (**Figure 4A**) was downregulated. Groα levels were also quantified in cell media, reflecting the differential expression of the cytokine in Calu-3 and H2228 cells (**Figure 4B**). These results suggest that STAT1 is an important player in the production of cytokine mediators involved in paracrine communication, as its silencing suppresses the expression of cytokines typically present in an immunosuppressive environment.

Furthermore, the content of EVs was investigated as a potential source of paracrine signals. EVs were isolated from WT and STAT1-silenced Calu-3 and H2228 cells, and they were characterized according to the International Society of Extracellular Vesicles (ISEV) indications (**Figure 5**). As per Nanoparticle Tracking Analysis (NTA) results, EVs from WT and silenced condition show different mean size, concentration and total particles number (**Figure 5A**), and they were also observed at the transmission electron microscope (TEM) (**Figure 5B**). Protein characterization of EVs was carried out by checking the expression of typical EVs markers, such as TSG101, Alix, Actinin-4, and Annexin XI. Cytochrome C was used to exclude the presence of protein contaminants (**Figure 5C**). Furthermore, proteomic analysis was conducted on the content of EVs isolated from H2228 cells: beside showing the expression of various typical EVs markers (**Figure 6A**), and so confirming their correct isolation, the analysis also revealed the presence of STAT1, whose abundance reflects its silencing in the cellular counterpart, as well as the presence of Groα, which was detected in EVs from WT cells but not in EVs from STAT1-silenced cells (**Figure 6B**), opening at the possibility of STAT1 and cytokines to be mobilized out of tumor cells in the cargo of EVs.

Overall, these results suggest that STAT1-dependent chemo-immuno-resistance may act through paracrine signals, such as cytokine release and EVs, leading to the reshape of the tumor immune-environment.

**A**

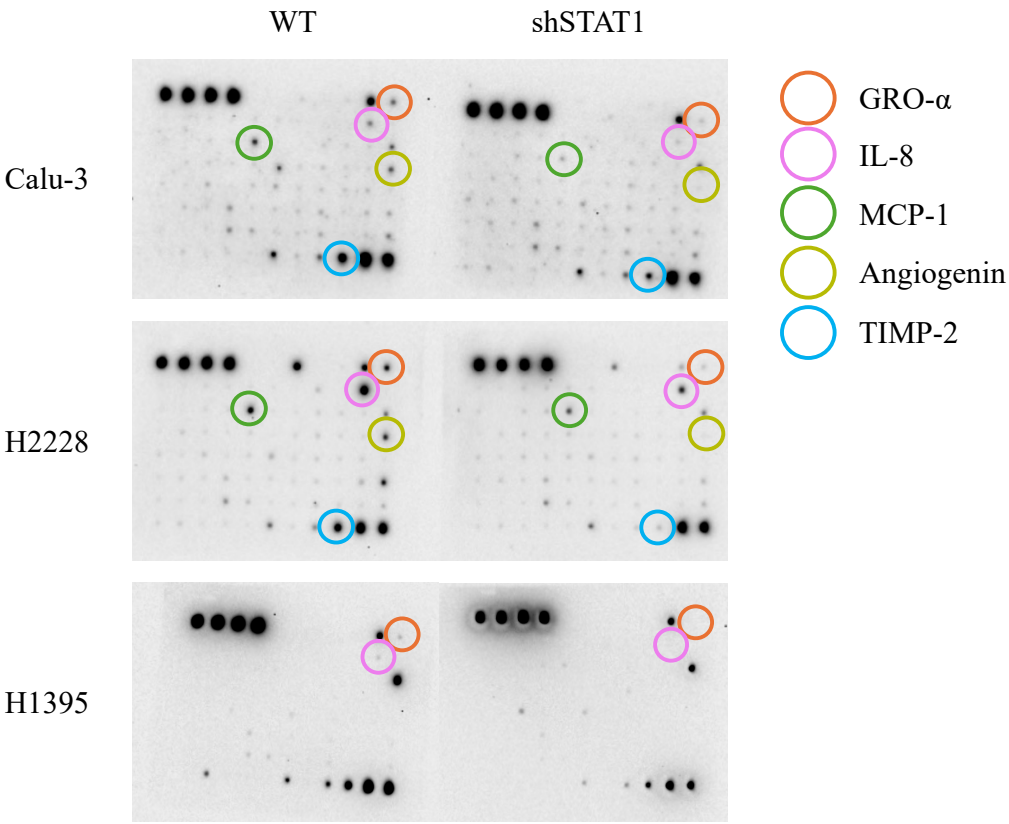


**B**

| Sample | µg/ml |
|---|---|
| Calu-3 WT | 0,000565407 |
| Calu-3 shSTAT1 | 0,000410222 |
| H2228 WT | 0,000759296 |
| H2228 shSTAT1 | 0,000636333 |

***Figure 4***. The potential role of paracrine signals: cytokines. Differential expression of cytokines in WT and silenced (shSTAT1) Calu-3, H2228 and H1395 cells (A). All cell lines show a downregulation of Groα (CXCL1; circled in orange) and IL-8 (CXCL8; circled in pink), while only Calu-3 and H2228 also show a decreased expression of MCP-1 (CCL2; circle in green), Angiogenin (circled in yellow), and TIMP2 (circled in light blue). Pictures are representative of one of two independent experiments. Quantification (B) expressed as µg/ml of Groα released from Calu-3 and H2228 cells.

**A**

WT shSTAT1

Calu-3

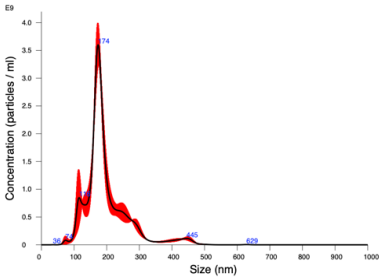


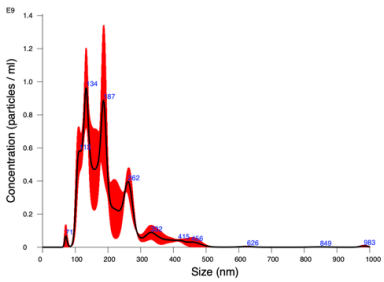


H2228

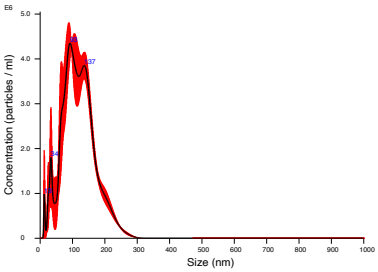


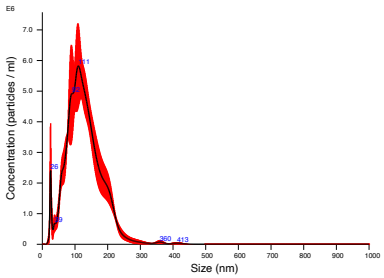


| Sample | Mean size (nm) | Accurate particles concentration (particles/ml) | Number of isolated EVs |
|---|---|---|---|
| **Calu-3 WT** | 199,3 | 3,46E+13 | 8,86E+12 |
| **Calu-3 shSTAT1** | 204,83 | 2,12E+13 | 7,83E+12 |
| **H2228 WT** | 127,5 | 8,63E+11 | 1,76E+11 |
| **H2228 shSTAT1** | 122,07 | 6,32E+11 | 1,29E+11 |

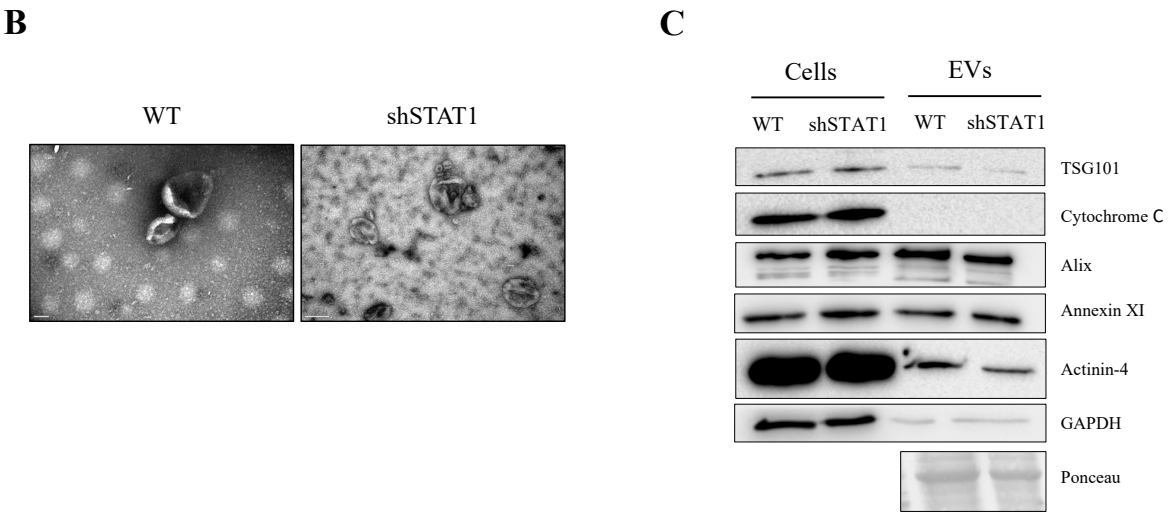


***Figure 5***. EVs characterization. Nanoparticle Tracking Analysis (NTA) data, including EVs mean size, accurate particles concentration and number of isolated EVs (A) of 100k EVs isolated from WT and STAT1-silenced Calu-3 and H2228 cells, showing their mean size and concentration. EVs visual characterization (B): morphology of EVs from WT and STAT1-silenced H2228 cells obtained with transmission electron microscope; magnification is set to 100 nm. Immunoblot (C) showing typical markers of EVs (TSG101, Cytochrome C, Alix, Annexin XI, Actinin-4). GAPDH was used as control of equal protein loading for cell lysates, while ponceau staining was used as control of equal protein loading for vesicles. Pictures are representative of one of three independent experiments.

**A**

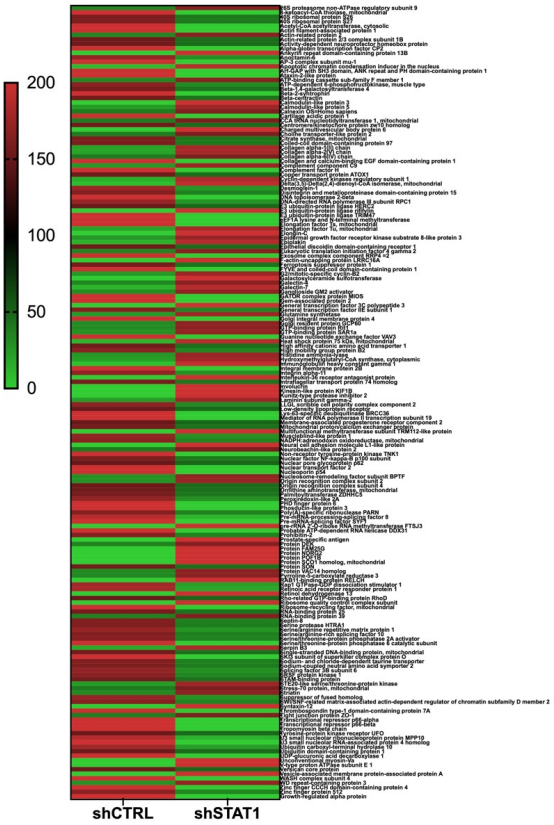


**B**

| *Accession Number* | *Protein Description* | *% of Abundance (WT/shSTAT1)* |
|---|---|---|
| | ***Main proteins EVs-related*** | |
| Q99816 | Tumor susceptibility gene 101 protein (TSG101) | 37.92/30.44 |
| Q8WUM4 | Programmed cell death 6-interacting protein (Alix) | 103.12/99.99 |
| O43707 | Alpha-actinin-4 | 21.33/18.39 |
| P07355 | Annexin A2 | 20.17/15.74 |
| P08758 | Annexin A5 | 36.44/74.64 |
| P08133 | Annexin A6 | 73.33/92.98 |
| P04406 | Glyceraldehyde-3-phosphate dehydrogenase (GAPDH) | 60.86/60.36 |
| P21926 | CD9 antigen | 86.79/93.73 |
| P08962 | CD63 antigen | 72.41/60.53 |
| P60033 | CD81 antigen | 105.85/88.99 |
| | ***Cytokines*** | |
| P09341 | Growth-regulated alpha protein (GROα) | 200/0 |
| P16035 | Metalloproteinase inhibitor 2 (TIMP-2) | 96.8/103.2 |
| | ***STAT1*** | |
| P42224 | Signal transducer and activator of transcription 1-alpha/beta (STAT1) | 120.4/79.6 |

***Figure 6***. Proteomic analysis of 100k EVs released by WT and STAT1-silenced H2228 cells. Heatmap data (**A**) of the protein profile of EVs, and table (**B**) presenting the main proteins (accession number, protein description, percentage of abundance) commonly present in EVs, as well as STAT1 and cytokines presence. Proteomics analysis included data from three independent experiments.

### 4.5 Ferrocenyl-erlotinib conjugates are active against erlotinib-resistant NSCLC cells *in vitro*

In this thesis, the resistance of NSCLC to target therapies, specifically EGFR inhibitors, was also addressed. Five different Erlotinib-derived synthetic compounds containing a ferrocene group (**Figure 7A**), produced in collaboration with the department of Organic Chemistry, Faculty of Chemistry, University of Łódź in Poland, were screened in both Erlotinib-sensitive (A549, H1395) and Erlotinib-resistant (H1650, H1975) NSCLC cells as well as against non-tumoral bronchial epithelium (BEAS-2B) cells. Determined IC50 concentrations after 48 h treatment time are shown in **Table 1**. The higher activity, compared to Erlotinib, of the majority of these compounds against Erlotinib-resistant H1650 (presenting loss of PTEN) and H1975 (harboring the T790M mutation in EGFR gene) cells prompted us to focus our studies on these two cell lines.

To compare cytotoxicity of all compounds and erlotinib in erlotinib-resistant lung cancer cell lines, cells were incubated with 20 μM concentration of each compound for 24h, 48h and 72h. Effects of erlotinib and derivative compounds on cell viability after 24h were moderate, only compound 3 caused about 20% of cancer cells death. After 48h H1650 and H1975 cell viability was decreased to 80% in case of erlotinib and compound 2 to about 50% in erlotinib-resistant lung cancer cells treated with compounds 3, 5, 6. After 72h, erlotinib decreases cell vitality to 50% and compound 2 to about 25-35%, compounds 5 and 6 to about 20-25%. The most efficient at all time points was compound 3 decreasing erlotinib-resistant cell lines viability to 15-20% after 72h of incubation. Of note, compound 3 was the only one significantly cytotoxic after 24h (**Figure 7B**). Due to the nature of compounds that were created by addition to the erlotinib structure of a ferrocene group, the release of reactive oxygen species (ROS) was measured. As expected, due to iron presence, all investigated compounds were producing ROS. Compounds 2, 3, 5, 6 were producing significantly more ROS than erlotinib in both investigated cell lines, differently to compound 4 that produced more ROS than erlotinib only in H1975 cell line; the most efficient ROS producer was compound 3 (**Figure 7C**).

**A**

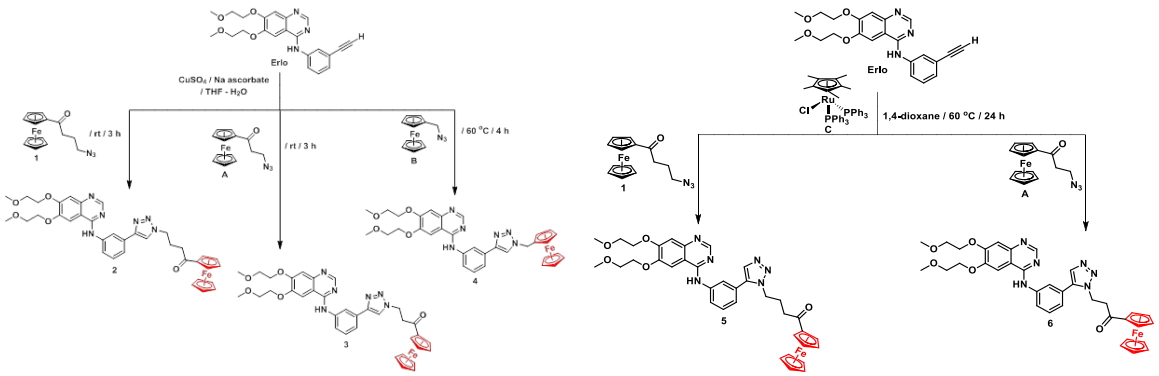


**B**

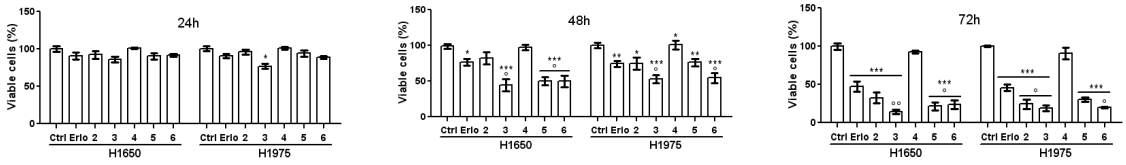


**C**

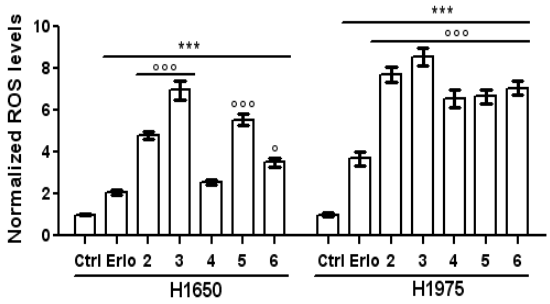


Figure 7. Ferrocenyl-erlotinib conjugates are active against erlotinib-resistant NSCLC cells *in vitro*. (A) Molecular structure of ferrocenyl-erlotinib Compounds 2-6. These compounds contain a ferrocene group, which is expected to release reactive oxygen species. (B) Cell viability was measured spectrophotometrically in triplicates. Data are means ± SD (n = 3). (C) ROS production was measured by a fluorimetric assay in duplicates. Data are means ± SD (n = 3). *p < 0.05, **p<0.01, **p<0.001: drugs treated cells vs. respective untreated (Ctrl) cells; °p < 0.05, °°p < 0.01, °°°p < 0.001: compounds treated cells vs. Erlo treated cells.

| | Erlo | 2 | 3 | 4 | 5 | 6 |
|---|---|---|---|---|---|---|
| **H1650** | 40 ± 0.16 | 761 ± 0.13 | 12 ± 0.13 | 228 ± 0.06 | 15 ± 0.05 | 18 ± 0.09 |
| **H1975** | 37 ± 0.08 | 26 ± 0.10 | 27 ± 0.08 | 312 ± 0.04 | 48 ± 0.06 | 27 ± 0.10 |
| **H1395** | 33 ± 0.11 | 359 ± 0.03 | 15 ± 0.11 | 355 ± 0.04 | 11 ± 0.08 | 18 ± 0.07 |
| **A549** | 12 ± 0.09 | 88 ± 0.04 | 7.9 ± 0.10 | 351 ± 0.05 | 42 ± 0.05 | 17 ± 0.04 |
| **BEAS-2B** | 74 ± 0.10 | 84 ± 0.96 | 155 ± 0.94 | 778 ± 0.18 | 121 ± 0.08 | 136 ± 0.11 |

***Table 1***. Cytostatic activity (IC50; μM) of compounds 2–6 and Erlotinib (Erlo) against Erlotinib-sensitive (A549, H1395) and Erlotinib-resistant (H1650, H1975) human lung cancer cells as well as against non-tumoral human bronchial epithelium (BEAS-2B) cells. Results are expressed as means ± SD of three independent experiments in four repeats each. IC50 was defined as the concentrations of compound that is required to achieve a 50% decrease in cell viability when compared to the viability of untreated control cells. Treatment time 48 h.

### 4.6 Erlotinib-derivative Compound 3 is more effective than Erlotinib in Erlotinib-resistant NSCLC cell lines

Among erlotinib-derived inhibitors, Compound 3 is the one with the highest cytotoxicity in erlotinib-resistant lung cancer cells, and this led to the hypothesis that at least part of the anticancer effect of those compounds, in particular compound 3, is caused by ROS-mediated oxidative stress. Of note, massive ROS production may lead to DNA damage[56] and destabilization in mitochondrial membrane potential in consequence leading to mitochondria destruction and finally to cell death[57]. For this reason, we evaluated the effect of compound 3 on cell cycle progression and compared it to erlotinib. Both erlotinib and compound 3 caused accumulation of cells in sub-G1 phase characterized by cell shrinkage and reduction in cell volume, in addition erlotinib - but not compound 3 - blocked cells in G0/G1 phase. Instead, compound 3 inhibited cells in the G2/M phase showing the difference in the mechanism of actions of both drugs (**Figure 8A**).

DNA damage is one of the main factors that contribute to G2/M arrest and indeed DNA damage was caused by compound 3: as expected, compound 3 caused significantly more DNA damage then erlotinib as demonstrated by positivity on pH2AX staining, chosen as indicator of DNA double-strand breaks inside the cells (**Figure 8B**). This DNA damage caused massive apoptosis rather than necrosis as demonstrated by Annexin V cell positivity in compound 3-treated erlotinib-resistant lung cancer cell lines but not in those treated with erlotinib, where the quantity of apoptotic cells is significantly lower (**Figure 8C**).

Moreover, compound 3 reduced mitochondrial membrane potential (**Figure 8D**) and subsequent intrinsic apoptosis activation as shown by activation of mitochondrial caspases 9 and 3 (**Figure 8E, 8F**). Therefore, erlotinib-resistant NSCLC cell lines death after compound 3 incubation was caused by DNA and mitochondrial damage, as a consequence of massive ROS production induced by compound 3. Indeed, co-incubation of N-acetyl cysteine (NAC), a ROS scavenger, with compound 3 or erlotinib decreased the quantity of ROS present inside the cells (**Figure 8G**) leading also to significant increase of erlotinib resistant lung cancer cells survival (**Figure 8H**) demonstrating that the additional activity of compound 3 compering to erlotinib against cancer cells was mostly dependent from massive ROS production and that it can be contrasted by addition of antioxidants.

**A**

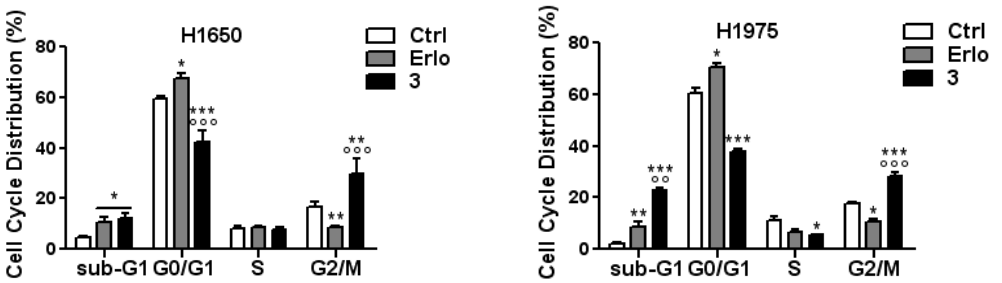


**B**

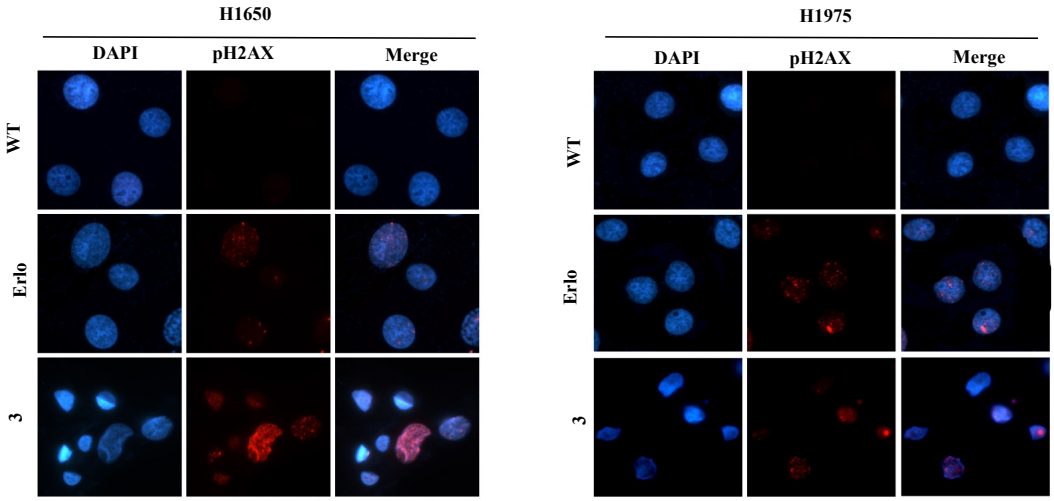


**C**

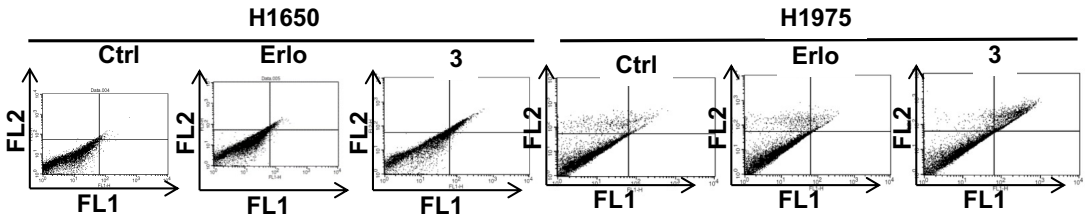


| | | UL | UR | LL | LR |
|---|---|---|---|---|---|
| H1650 | Ctrl | 0,51±0,5 | 0,96±0,13 | 98,33±0,14 | 0,2±0,51 |
| | Erlo | 2,7±0,16** | 4,04±0,25*** | 92,8±0,21** | 0,82±0,09 |
| | 3 | 3,17±0,28** | 14,18±0,66***°°° | 81,31±0,16*** | 0,88±0,05 |
| H1975 | Ctrl | 2,56±0,31 | 2,28±0,17 | 94,43±0,33 | 0,2±0,05 |
| | Erlo | 3,56±0,25 | 5,66±0,42*** | 90,49±0,72* | 0,82±0,09*** |
| | 3 | 2,64±0,03 | 12,9±1,13***°°° | 81,31±0,16*** | 0,88±0,05*** |

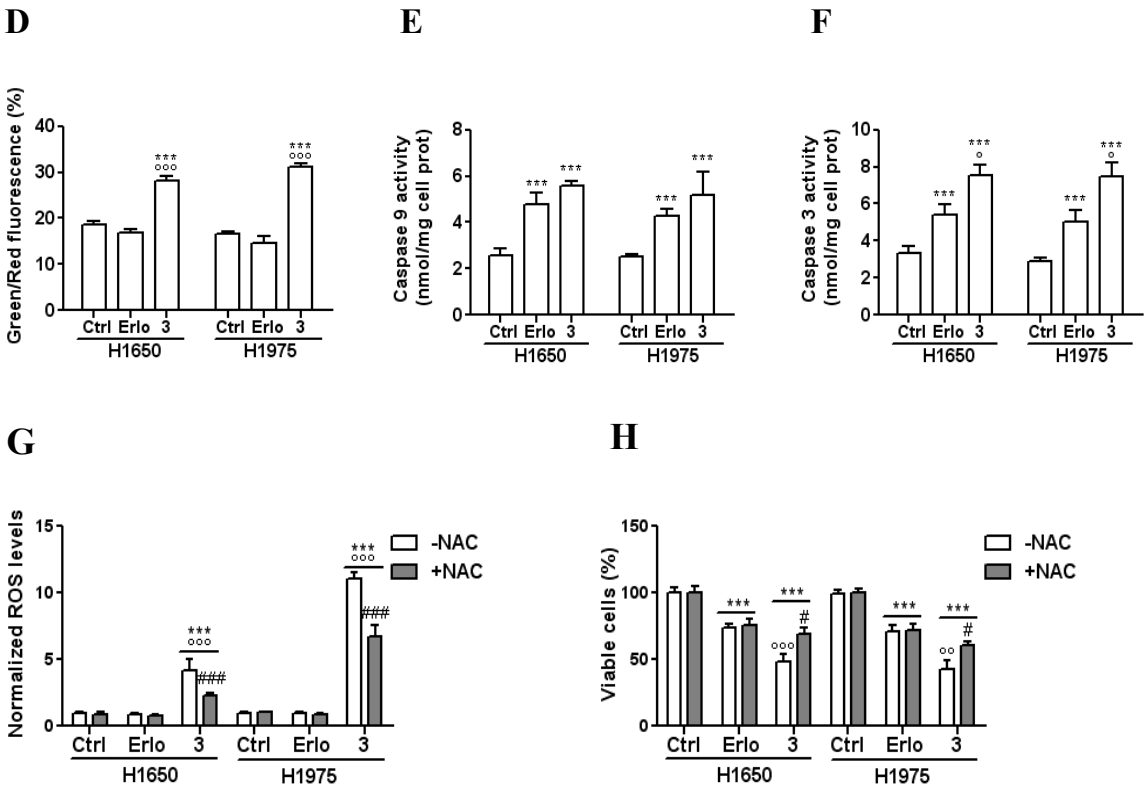


***Figure 8***. Erlotinib-derivative Compound 3 is more effective than Erlotinib in Erlotinib-resistant NSCLC cell lines. (A) Cell cycle distribution was measured by flow cytometry in duplicates. Data are means ± SD (n = 3). *p < 0.05, **p<0.01, **p<0.001: drugs treated cells vs. respective untreated (Ctrl) cells; °°p < 0.01, °°°p < 0.001: compound 3 treated cells vs. Erlo treated cells. (B) DNA damage was measured by staining cells with anti-pH2AX antibody. Nuclei were counter-stained with DAPI. Scale bar: 10 μm. (10x ocular, 100x objective). At least 10 fields were examined for each condition. The Figure is representative of 1 out of 3 experiments with similar results. (C) Cell apoptosis was measured by flow cytometry in duplicates. Data are means ± SD (n = 3). *p < 0.05, **p<0.01, **p<0.001: drugs treated cells vs. respective untreated (Ctrl) cells; °°°p < 0.001: compound 3 treated cells vs. Erlo treated cells. (D) Mitochondrial damage was measured by a fluorimetric assay in duplicates using JC-1 dye. The percentage of green versus red mitochondria was considered a marker of mitochondrial depolarization. Data are means ± SD (n = 3). ***p<0.001: drugs treated cells vs. respective untreated (Ctrl) cells; °°°p < 0.001: compound 3 treated cells vs. Erlo treated cells. (E, F) The activity of caspase 9 and caspase 3 was measured by a fluorimetric assay in duplicate in the cytosolic extracts. Data are means ± SD (n = 3). ***p<0.001: drugs treated cells vs. respective untreated (Ctrl) cells; °p < 0.01: compounds treated cells vs. Erlo treated cells. (G) ROS production was measured by a fluorimetric assay in duplicates. Data are means ± SD (n = 3). ***p<0.001: drugs treated cells vs. respective untreated (Ctrl) cells; °°°p < 0.001: compound 3 treated cells vs. Erlo treated cells; ###p< 0.001: drugs+NAC treated cells vs. drugs treated cells. (H) Cell viability was measured spectrophotometrically in triplicates.

Data are means ± SD (n = 3). ***p<0.001: drugs treated cells vs. respective untreated (Ctrl) cells; °°p < 0.001, °°°p < 0.001 compound 3 treated cells vs. Erlo treated cells; #p< 0.001: drugs+NAC treated cells vs. drugs treated cells.

## 5. Discussion

NSCLC is the leading cause of cancer-related mortality worldwide. Despite the development of new therapeutic strategies, which have significantly improved both the prognosis and quality of life for patients with NSCLC, lung cancer remains challenging to treat due to its high recurrence rate. One of the main reasons for this recurrence is the development of resistance to therapy. Several mechanisms are involved in the development of drug resistance, including the presence of genetic mutations that alter drug targets, the activation of alternative signaling pathways, and the tumor's ability to adapt its microenvironment. Additionally, cancer stem cells, immune evasion, and increased drug efflux are key contributors. The complex nature of NSCLC's biology means that even with advancements in precision medicine, targeted therapies, and immunotherapy, overcoming drug resistance remains a major obstacle in improving patient outcomes[26,27,28].

The first part of this thesis investigated the intricate mechanisms underlying chemoresistance and immunoresistance in NSCLC. A particular focus is placed on one of the leading pathways involved in drug resistance, the JAK/STAT signaling pathway, which plays a critical role in cancer cell survival, proliferation, and immune evasion[47].

The JAK/STAT pathway was identified as a leading pathway of resistance in NSCLC cell lines, notably highlighting an important expression of STAT1 at the mRNA and protein level. As part of the JAK-STAT signaling pathway, STAT1 is typically activated in response to interferons and other cytokines, promoting immune responses and cellular stress resistance. In NSCLC, however, overexpression or hyperactivation of STAT1 can lead to enhanced DNA repair mechanisms, increased survival signaling, and the promotion of an immunosuppressive tumor microenvironment. These factors collectively contribute to resistance against apoptosis induced by therapies and can enable tumor cells to evade immune detection, complicating treatment outcomes[46,47]. The effect of STAT1 silencing was evaluated in three different NSCLC lines, selected based on their basal levels of STAT1 and PD-L1, as studies have shown that STAT1 can drive the upregulation of PD-L1 in NSCLC cells, especially in response to IFN-γ, contributing to an immunosuppressive tumor microenvironment and allowing cancer cells to escape immune surveillance[49]. The interplay between PD-L1 and STAT1, particularly in the context of immune evasion and cancer progression, is not a prerogative of NSCLC but has been investigated in other tumors as well. In hepatocellular carcinoma, hexokinase domain

component 1 (HKDC1) promotes tumor immune evasion in a $CD8^+$ T cell-dependent manner by activating STAT1/PD-L1 in tumor cells[58], and in melanoma the eukaryotic translation initiation complex (eIF4F), which correlates with the response to immunotherapy in this type of cancer, regulates the expression of IFN-γ-induced PD-L1 on cancer cells by regulating translation of STAT1[59]. Furthermore, in squamous cell carcinomas (SSCs), where immunotherapy using PD-1/PD-L1 antibodies has been approved in advanced stages, it has been shown that TP63 suppresses the IFN-γ signaling by inhibiting the transcription of STAT1, and so impeding $CD8^+$ T-cells infiltration, tumor killing and so decreasing the efficacy of PD-1 blockade[60]. All these examples show how PD-L1 expression is regulated by the JAK/STAT pathway via the IFN-γ signaling. IFN-γ, secreted by NK cells, binds to the IFN-γ receptor to initiate signaling, inducing phosphorylation and activation of JAK1/2, and recruiting STAT members, including STAT1. Once recruited, the STATs are activated, forming a dimer that allows them to translocate into the nucleus and bind to the IFN-γ-inducible gene promoter region. The regulation of PD-L1 by STAT1 can happen directly, when it binds the IFN-activated sequence on PD-L1 promoter, or indirectly, either via the secretion of cytokines, such as IL-6, which activate STAT members or the binding of STAT1 itself to the gamma activated sequences (GAS), resulting in transcription of interferon-stimulated genes (ISGs), which include antigen processing and presentation factors (B2M, CD74, PSMB9, LAP3), immune response-related transcription regulators (IRF1, IRF7, SP110, BATF2), chemokines and cytokines (CXCL10, CXCL11, IL15). In addition, another indirect mechanism was identified in SCLC and ovarian cancer and is represented by the IFN-induced activation of the transcription factor interferon regulatory factor 1 (IRF1), which binds STAT1. The STAT1-IRF1 complexes, in turn, bind to the GAS elements or bind PD-L1 promoter itself[60,61,62,63].

Unexpectantly, this work did not show any STAT1-dependent variation in PD-L1 expression, but T-lymphocytes co-cultured with NSCLC were found to be more active against STAT1-silenced cells than WT cells, and in one case – T-cells co-cultured with STAT1-silenced H2228 cells – a higher proliferation of lymphocytes was observed. T-cells co-cultured with Calu-3 or H1395 did not show the same trend, although it was possible to observe a reduction of cell viability. T-cell activation is a crucial process in the immune response against NSCLC, playing a central role in anti-tumor immunity: NSCLC tumors often develop mechanisms to suppress T-cell activation, such as upregulating immune checkpoint proteins on T-cells and inhibit their function[64]. Overcoming these inhibitory signals through therapies such

as immune checkpoint inhibitors, has become a key strategy in enhancing T-cell activation and improving immune-mediated tumor destruction in NSCLC. Moreover, STAT1 impairment reflects greatly on other immune cells besides T-cells: STAT1 is essential for NK cell maturation and NK cell-dependent tumor surveillance, and the lack of STAT1 was demonstrated to decrease NK cells-mediated cytotoxicity *in vivo*[65].

Considering the role of STAT1 in immunoresistance, its importance was also evaluated in chemoresistance. It is known that STAT1 can promote resistance by enhancing the cancer cell's ability to repair DNA damage induced by chemotherapeutic agents, thus preventing apoptosis. Additionally, STAT1 activation supports the expression of anti-apoptotic proteins and can modulate the tumor microenvironment to become more immunosuppressive, further reducing the efficacy of chemotherapy. By increasing the survival and repair mechanisms of tumor cells, STAT1 contributes to a reduced response to chemotherapy, making it a potential target for improving treatment outcomes in chemotherapy-resistant cancers[47,48]. In renal cell carcinoma, knock-down of STAT1 led to a sensitization of tumor cells to paclitaxel *in vitro*, with significant downregulation of DNA damage-related genes such as GADD45A and MAP2K6[66], and in ovarian cancer acetylation of STAT1 by histone deacetylase 4, which prevents the phosphorylation and activation of STAT1, sensitized tumor cells to cisplatin *in vitro*[67]. Moreover, the presence of STAT1 in stromal cells may represent another source of variation in chemotherapy response: in a study published by Zellmer and colleagues, depletion of STAT1 in cancer-associated fibroblast (CAFs) impaired early breast cancer progression *in vivo* and inhibition of STAT1 in combination with doxorubicin, increased therapeutic efficacy in treating mouse mammary gland tumors[68]. Indeed, in this work, STAT1-silenced cells showed higher chemosensitivity to cisplatin, paclitaxel and combination therapy.

Given that PD-L1 expression remained unaltered after STAT1 silencing and chemosensitivity was restored in conditions of exchanged media between WT and shSTAT1 cells, it was hypothesized that the STAT1-mediated chemo-immunoresistance could be due to paracrine mechanisms and soluble factors, such as chemokines and cytokines. Chemokines binding their respective receptors cause the activation of signaling pathways involved in normal inflammatory response when their expression is physiological. Instead, aberrant chemokine expression causes abnormal inflammatory reactions, leading to constitutive activation of oncogenes and inactivation of tumor suppressor genes, as usually occurs in TME[69].

Indeed, this thesis work evaluated the differential expression of cytokines in WT and STAT1-silenced cells. Two cytokines, Groα and IL-8 were found commonly downregulated in all three STAT1-silenced NSCLC cell lines.

IL-8 is a proinflammatory chemokine secreted by macrophages and endothelial cells, whose receptors are found on monocytes, granulocytes, and endothelial cells. Its production is dependent on upstream NF-kB signaling, as well as the JAK/STAT pathway, and the chemokine itself triggers downstream activation of PI3K and MAPK signaling cascades. IL-8 is known to influence the biology of numerous types of tumors, including lung cancer, specifically by participating in processes such as epithelial-to-mesenchymal transition (EMT) and angiogenesis, and IL-8-dependent signaling heavily modifies the TME, as it induces the conversion of resident monocytes into tumor-associated macrophages (TAM) and recruits myeloid derived suppressor cells (MDSC), enabling suppression of the anti-tumor efficacy of cytotoxic T-cells[70,71]. Different studies show that IL-8 can induce resistance to chemotherapeutic agents, such as doxorubicin in colorectal cancer (CRC) and osteosarcoma[72,73], and to cisplatin in gastric cancer and malignant pleural mesothelioma[74,75], and it can also participate in resistance to ICI such as the PD-1/PD-L1 and CTLA-4, as it was shown by studies on melanoma and NSCLC patients[70].

Groα, also known as CXCL1, is a chemokine physiologically involved in inflammatory reactions in various ways, including the stimulation of angiogenesis and the recruitment of neutrophils. In tumors, Groα is produced in the tumor by cancer cells, CAFs, MDSCs, mesenchymal stem cells (MSCs) and tumor-associated macrophages (TAMs) and, acting as a chemo-attractant for tumor-associated immune cells, it is known to increase tumor proliferation, cancer cell migration, and EMT[76]. The role of Groα in therapy resistance still needs to be thoroughly explored, but some studies indicate that this cytokine may be involved in the onset of chemotherapy resistance. Groα was linked to temozolomide resistance in glioblastoma and to paclitaxel resistance in melanoma, in which the cytokine levels seem to increase as a result of the treatment itself, leading to increased chemoresistance and metastasis development[77,78]. This was demonstrated also in the case of paclitaxel and carboplatin in melanoma and in breast cancer treated with paclitaxel and docetaxel[78,79]. Moreover, blocking of CXCR2, Groα main receptor, enhanced chemotherapeutic response, suppressed tumor growth, angiogenesis, and metastasis in NSCLC[80].

As demonstrated in several studies on breast cancer, chemotherapy itself determines the release of factors from the stromal environment that induce Groα production and release from cancer cells through the NF-κB/JAK/STAT axis: when Groα is released from cancer cells, it recruits myeloid cells responsible for the secretion of other paracrine factors that support tumor growth through the triggering of pro-survival pathways and selection of resistant cancer cells, making the chemo-induced cytokine storm one of the factors related to the shaping of TME and chemoresistance[81]. Further studies, supporting the involvement of Groα in shaping the immune TME, concern pancreatic adenocarcinoma mouse models in which the ablation of the Groα gene led to increased $CD8^+$ T-cells infiltration in TME, promoting the anti-tumoral functions and response to immunotherapy[82]. Although these implications have not been demonstrated in NSCLC cells yet, it is known that Groα promoter is directly bound by STAT1[76], and given that this thesis work displayed the downregulation of Groα in all STAT1-silenced NSCLC cell lines, it is possible to hypothesize that similar mechanisms involving this cytokine occur in lung cancer as well.

Another source of paracrine signals is represented by EVs. EVs are bioactive cargos that carry lipids, genetic material, growth factors, and signaling molecules involved in promoting a variety of different biological mechanisms. EVs work as a shuttle to allow communication between cancer cells and the TME, holding the potential to elicit TME reprogramming. At the same time TME also affects tumor cells through EVs, which can result in either tumor promotion or inhibition[83]. In NSCLC, EVs promote cell proliferation and metastasis, enhance cancer progression and drug resistance, allowing cancer cells to evade the immune response[84]. By creating an immunosuppressive microenvironment, EVs have a crucial role in establishing "cold" tumors, or tumor less responsive to immunotherapy and chemotherapy. Oncosomes, or EVs released by cancer cells carrying oncoprotein and genetic materials, have a pivotal role in shaping the TME and reprogramming healthy and stromal cells. Chemokines, secreted by tumoral stroma, recruit myeloid-derived suppressor cells (MDSCs), and together with oncosomes they downregulate Natural Killer (NK) cells and T-cell activity. Moreover, cancer cells also release PD-$1^+$ EVs mediating immunotherapy resistance. All these factors contribute to the immunosuppressive TME. Furthermore, cancer EVs are responsible for chemoresistance as well as they can efflux platinum-based drugs out of cancer cells either by transporting small molecule regulators, such as miRNA, into tumor cells, and so influencing drug efflux

transporters and increasing the drug efflux itself, or they can embed drugs and expel them from tumor cells[83,85].

EVs are also known to influence the immune response in cancer by promoting the differentiation of various cell types into pro-tumorigenic, immunosuppressive, anti-inflammatory, and chemoresistant phenotypes. These include the differentiation of fibroblasts into CAF, monocytes and TAM into M2-polarized TAM, and neutrophils into N2-polarized neutrophils[86]. Moreover, vesicles are able to induce apoptosis in DCs and CD8+ T-cells, and to disable NK cells: for example, PTEN-enriched EVs appeared to regulate the PI3K/AKT pathway, leading to AKT dephosphorylation and increasing the expression of pro-apoptotic BAX and decreasing antiapoptotic Bcl-2, Bcl-xL, and myeloid leukemia cell differentiation protein in activated killer T cells[85], while in prostate cancer-derived EVs express ligands for NK group 2 member D (NKG2D), a transmembrane receptor that mediates T-cell receptor activation and the direct killing of targets from immune cells, which selectively decrease the expression of the receptor NKG2D on NK and CD8+ T-cells, leading to impaired cytotoxic function of these immune cells and tumor immune escape[87].

Both cytokines and EVs are systems that allow communication between cells, and it is interesting to note that they often work together, as cytokines can be encapsulated in vesicles and transported from one cell to another, both in physiological and pathological conditions. EVs can carry different cytokines, either on their surface or in their cargo, so that these molecules are protected from enzymatic degradation in the extracellular environment and can be delivered to distant cells. Commonly EVs-transported cytokines include TNF, many interleukins, CCL2, transforming growth factor-β (TGFβ), and even Groα itself, which is usually found on the vesicles' surface[88]. In triple-negative breast cancer (TNBC) it was observed that Groα-enriched EVs are released at high levels from apoptotic cancer cells as a consequence of paclitaxel treatment, which leads to chemoresistance and metastasis[89]. Moreover, in another work on TNBC, when the amount of Groα in these vesicles is reduced, tumor cells are re-sensitized to paclitaxel-based chemotherapy *in vivo*[90].

In this work, EVs from WT and STAT1-silenced H2228 and Calu-3 cells were isolated, characterized and their content was investigated. It was found not only that STAT1 is carried in the cargo of EVs but that its abundance reflects STAT1-silencing in the cellular counterpart. Moreover, the same results were confirmed for Groα, which is downregulated in EVs released

from STAT1-silenced cells. Thus, Groα-enriched EVs could be used from NSCLC cells as a vehicle to communicate with other TME cells to favor tumor growth and immune escape.

Targeting STAT1 directly may result to be less beneficial than intended, as it is involved several biological pathways, in healthy cells as well as cancer cells. For this reason, the possibility to act downstream of STAT1, or on the paracrine signals it controls, should be considered. For example, targeting cancer-released cytokines could represent a valuable approach, as the use of neutralizing antibodies has already been employed[91], as well as engineering EVs to carry anti-tumoral signals. Considering the poor prognosis of the high chemokines-releasing NSCLC cases, the combination of CXCR2 (Groα receptor) inhibitors and chemotherapy could be a potential therapeutic approach to improve patients' response, but further studies are needed to apply it in a clinical setting. Nevertheless, targeting the immune microenvironment appears to be promising due to the potentially low selective pressure for mutations and epigenetic changes on the stroma compared to tumor genomes[82].

Overall, these results on STAT1's involvement in chemo-immuno-resistance may have important implications in NSCLC oncology, as its expression could be considered as a potential biomarker for tumor prognosis and early onset of resistance, and its manipulation could be exploited to increase chemosensitivity and immune-killing by T-cells, with the aim of overcoming these simultaneous resistances.

In a second part, this thesis also addressed resistance to target therapy in NSCLC: screening of anticancer activity studies of the ferrocenyl-erlotinib compounds was carried out against erlotinib-sensitive A549 and H1395 as well as erlotinib-resistant H1975 and H1650 NSCLC cells. This compounds figure as ferrocenyl-compounds, carrying a ferrocenyl (Fc) entity which activates oxidation-related mechanism of action, typical of other organometallic anti-cancer compounds. The most relevant example of Fc-derived anticancer drugs are ferrocifens, whose structure was first obtained from the substitution of the phenyl ring in the anti-breast cancer drug tamoxifen with the Fc entity: while tamoxifen shows activity solely against estrogen receptor positive (ER+) breast cancer, the ferrocifens are active against both ER+ and ER- tumors. In ferrocifens, the Fc group can undergo a one-electron oxidation producing the corresponding ferrocenium radical cation, in a reversible reaction that has important biological applications, since the ferrocenium ion can generate ROS under physiological conditions. The ability for ROS generation makes the Fc group a redox-active, cytotoxic entity with many potential bio-applications, including anticancer agents[92,93].

In this work, ferrocenyl compounds 2-6 were synthetized as erlotinib-derivatives, through a metal-catalyzed azide-alkyne 1,3-dipolar cycloaddition (click) reaction. This reaction is relatively simple in execution, can be carried out in complicated matrixes including living cell environment, with little or no byproducts, and it was already established to produce erlotinib derivatives with anticancer activity[94]. Among the five tested compounds, compound 3 and 6 showed higher cytotoxic activity against erlotinib-sensitive as well as erlotinib-resistant cancer cells compared to erlotinib, and notably, they also showed low activity against non-cancerous human bronchial epithelium BEAS-2B cells. Indeed, compared to the other compounds, compound 3 and compound 6 have C(=O)CH2CH2 linker between the ferrocenyl and the triazole rings[95], suggesting that their higher anticancer activity is mainly dependent upon the type and length of the linker between these two entities.

Oxidative stress and ROS induction have been recognized as key factors that contribute to the anticancer activity of organometallic compounds, defined as molecules with a distinct metal-carbon bond. Besides ferrocenyl-derived compounds, other research-relevant organometallic compounds include gold complexes and ruthenium complexes, which are still being tested many different cancers, such as breast, lung, and colorectal cancer[96,97,98].

Indeed, this work revealed that all ferrocenyl compounds produced significantly more ROS than erlotinib, with compound 3 producing the most ROS out of all tested compounds, and so suggesting that the mechanism of action of these erlotinib-derivatives mainly relies in the induction of oxidative stress in cancer cells.

Excessive ROS production can directly damage DNA by causing mutations, strand breaks, and base modifications, which can compromise genomic integrity and lead to apoptosis. Additionally, high ROS levels can impair mitochondrial function: oxidative stress causes the activation of pro-apoptotic elements, such as members of the BCL2 family, which drive mitochondrial outer membrane permeabilization and the creation of the mitochondrial permeability transition pore, thus regulating the formation of pores in the outer mitochondrial membrane and reducing the mitochondrial transmembrane potential ($\Delta\Psi m$). This breach results in the release of more apoptotic molecules, such as cytochrome C, and in the activation of caspase-9 and subsequentially of caspase-3, one of the major players in the apoptosis process. Caspase-3-dependent apoptosis triggers a feedback loop where dysfunctional mitochondria produce even more ROS, further exacerbating oxidative damage. Mitochondrial ROS cause damage to mitochondrial structures themselves, such as mitochondrial DNA, leading to

disruptions in the transcription of proteins vital to the mitochondrial electron transport chain, and so inducing malfunction and hindering ATP synthesis. This, in turn, might increase ROS generation and escalate the mitochondrial permeability transition pore opening, ultimately causing mitochondria-driven apoptosis[57,99].

Indeed, results showed the activation of caspase-9 and -3, as well as mitochondrial transmembrane potential imbalance and DNA damage in cells treated with ferrocenyl compounds. Moreover, compound 3 was able to block cell cycle in G2/M phase, instead of G0/G1 phase as Erlotinib. Interestingly, the behavior of compound 3 is similar to classic chemotherapeutic drugs such cisplatin or doxorubicin, which both block cells in G2/M phase and also produce oxidative stress partially responsible for their anticancer activity[100,101].

Other erlotinib-derived compounds have been tested in different types of cancer, expanding the field of TKIs-derived organometallic compounds in cancer treatment. For example, derivatization of erlotinib with boron-cluster compounds has been successfully obtained and they were tested against EGFR-overexpressing glioblastoma cells *in vitro*, where conjugates showed high anticancer activity compared to erlotinib[102]. Moreover, biological activity of phosphane gold (I) complex of erlotinib was investigated in triple-negative breast cancer, and it was found that this conjugate's anticancer property is dictated by the phosphane gold entity and differs from that exhibited by erlotinib alone: whereas erlotinib acts as EGFR inhibitor, arresting cancer cells in G1 phase, its gold derivative relies on a different mechanism of action based on ROS production, and so mitochondrial potential imbalance, DNA scission and cell cycle arrest in S and G2/M phases[96], not differently from the ferrocenyl-conjugates analyzed in this work. Other erlotinib-derived compounds were tested on lung cancer *in vitro*: the 1,2,3-triazole conjugates, obtained via the *click* reaction by Mao and colleagues in 2022, exhibited remarkable antitumor activity than erlotinib, relying on cell death mechanisms such as mitochondrial apoptosis and cell cycle arrest[103].

It might be then speculated that the observed superior to erlotinib anticancer activity of compound 3 examined in this work arise as a combination of ROS induction and EGFR inhibition with the former mechanism being dominant over the latter, and so representing a mechanism of action independent from classical mechanisms of resistance to EGFR inhibitors.

## 6. Conclusion and future perspectives

This study investigates the role of JAK/STAT signaling pathway, a crucial driver of resistance mechanisms in many types of cancer, in the context of NSCLC. It identifies STAT1 as a central element within this pathway, contributing to clarify its debated role in the disease and demonstrating how it acts as a critical resistance factor against both immune response and chemotherapy.

This research project revealed that silencing STAT1 in NSCLC cells had important effects on the immune response toward these cells. With STAT1 inhibited, immune cells showed an enhanced ability to eliminate cancer cells, which suggests that STAT1 plays a suppressive role in T-lymphocytes activation. Notably, STAT1 suppression also altered the sensitivity of NSCLC cells to traditional chemotherapy, as cells lacking active STAT1 were less able to resist the toxic effects of chemotherapeutic agents, underlining STAT1's contribution to chemoresistance in NSCLC.

This thesis also uncovers a potential mechanism by which STAT1 promotes NSCLC resistance through its influence on cytokine production. Specifically, it identifies the immunosuppressive cytokine Groα, a transcriptional target of STAT1, as a key player in this resistance mechanism. The increased presence of Groα, driven by STAT1 activity, may contribute to creating a microenvironment that shields cancer cells from immune detection and destruction. Further analysis showed that both STAT1 and Groα are also packaged into EVs secreted by NSCLC cells. These EVs likely facilitate paracrine signaling, allowing cancer cells to influence neighboring cells and further enhance resistance through STAT1-mediated pathways. This finding reinforces the role of STAT1-dependent signaling in establishing a resistant tumor microenvironment.

The second part of the study focuses on the resistance against targeted therapies in NSCLC, particularly investigating compounds derived from erlotinib. This research identifies erlotinib derivatives with enhanced biological activity, which perform better in erlotinib-resistant NSCLC cells than erlotinib itself, and their mechanism of action based on oxidative stress, that remains effective despite the conventional resistance pathways that typically undermine EGFR inhibitors. This suggests that these new compounds could overcome some of the inherent limitations of traditional EGFR-targeted therapies.

Moreover, the findings open to the possibility of combination therapies. Given that these erlotinib-derived compounds act independently of classical resistance mechanisms, they could

be particularly effective when used in association with platinum-based chemotherapy agents. Platinum drugs, which work by inducing DNA damage and arresting the cell cycle, may complement the action of these novel erlotinib-derived compounds. Together, they could create a synergistic effect, amplifying therapeutic efficacy by exploiting dual mechanisms of cell damage and growth arrest.

In conclusion, this thesis deepens on the controversial role of STAT1 in NSCLC therapy resistance, proposing STAT1 and its downstream paracrine effectors as novel markers and potential therapeutic targets. Additionally, it presents a promising new approach to address resistance to EGFR inhibitors.

## 7. References


1. Leiter, A., Veluswamy, R. R. & Wisnivesky, J. P. The global burden of lung cancer: current status and future trends. Nat. Rev. Clin. Oncol. 20, 624–639 (2023).
2. Corrales, L. et al. Lung cancer in never smokers: The role of different risk factors other than tobacco smoking. Crit. Rev. Oncol. Hematol. 148, 102895 (2020).
3. Gandini, S. et al. Tobacco smoking and cancer: A meta-analysis. Int. J. Cancer 122, 155–164 (2008).
4. Xue, Y., Wang, L., Zhang, Y., Zhao, Y. & Liu, Y. Air pollution: A culprit of lung cancer. J. Hazard. Mater. 434, (2022).
5. Hill, W. et al. Lung adenocarcinoma promotion by air pollutants. Nature 616, 159–167 (2023).
6. Coté, M. L. et al. Increased risk of lung cancer in individuals with a family history of the disease: A pooled analysis from the International Lung Cancer Consortium. Eur. J. Cancer 48, 1957–1968 (2012).
7. Chen, Z., Fillmore, C. M., Hammerman, P. S., Kim, C. F. & Wong, K. K. Non-small-cell lung cancers: A heterogeneous set of diseases. Nat. Rev. Cancer 14, 535–546 (2014).
8. Liang, J., Guan, X., Bao, G., Yao, Y. & Zhong, X. Molecular subtyping of small cell lung cancer. Semin. Cancer Biol. 86, 450–462 (2022).
9. Meijer, J. J. et al. Small cell lung cancer: Novel treatments beyond immunotherapy. Semin. Cancer Biol. 86, 376–385 (2022).
10. Seguin, L., Durandy, M. & Feral, C. C. Lung Adenocarcinoma Tumor Origin: A Guide for Personalized Medicine. Cancers (Basel). 14, (2022).
11. Tsim, S., O'Dowd, C. A., Milroy, R. & Davidson, S. Staging of non-small cell lung cancer (NSCLC): A review. Respir. Med. 104, 1767–1774 (2010).
12. Herbst, R. S., Morgensztern, D. & Boshoff, C. The biology and management of non-small cell lung cancer. Nature 553, 446–454 (2018).
13. Golding, B., Luu, A., Jones, R. & Viloria-Petit, A. M. The function and therapeutic targeting of anaplastic lymphoma kinase (ALK) in non-small cell lung cancer (NSCLC). Mol. Cancer 17, 1–15 (2018).

14. Jančík, S., Drábek, J., Radzioch, D. & Hajdúch, M. Clinical Relevance of KRAS in Human Cancers. J. Biomed. Biotechnol. 150960 (2010).
15. Yan, N. et al. BRAF-Mutated Non-Small Cell Lung Cancer: Current Treatment Status and Future PerspecKve. Front. Oncol. 12, 863043 (2022).
16. Hirsch, F. R. et al. Lung cancer: current therapies and new targeted treatments. Lancet 389, 299–311 (2017).
17. Marino, F. Z. et al. Molecular heterogeneity in lung cancer: From mechanisms of origin to clinical implications. Int. J. Med. Sci. 16, 981–989 (2019).
18. Duma, N., Santana-Davila, R. & Molina, J. R. Non–Small Cell Lung Cancer: Epidemiology, Screening, Diagnosis, and Treatment. Mayo Clin. Proc. 94, 1623–1640 (2019).
19. Dasari, S. & Bernard Tchounwou, P. Cisplatin in cancer therapy: Molecular mechanisms of action. Eur. J. Pharmacol. 740, 364–378 (2014).
20. Ghosh, S. Cisplatin: The first metal based anticancer drug. Bioorg. Chem. 88, 102925 (2019).
21. Tan, N. et al. Navitoclax Enhances the Efficacy of Taxanes in Non–Small Cell Lung Cancer Models. Clin. Cancer Res. 17, 1394–1404 (2011).
22. Ramalingam, S. & Belani, C. P. Carboplatin/gemcitabine combination in advanced NSCLC. Oncol. Williston Park N 18, 21–26 (2004).
23. Guo, Q. et al. Current treatments for non-small cell lung cancer. Front. Oncol. 12, 1–19 (2022).
24. Zappa, C. & Mousa, S. A. Non-small cell lung cancer: Current treatment and future advances. Transl. Lung Cancer Res. 5, 288–300 (2016).
25. Ko, E. C., Raben, D. & Formenti, S. C. The Integration of Radiotherapy with Immunotherapy for the Treatment of Non-Small Cell Lung Cancer. Clin. Cancer Res. Off. J. Am. Assoc. Cancer Res. 24, 5792–5806 (2018).
26. Otano, I., Ucero, A. C., Zugazagoitia, J. & Paz-Ares, L. At the crossroads of immunotherapy for oncogene-addicted subsets of NSCLC. Nat. Rev. Clin. Oncol. 20, 143–159 (2023).
27. Yuan, M., Huang, L. L., Chen, J. H., Wu, J. & Xu, Q. The emerging treatment landscape of targeted therapy in non-small-cell lung cancer. Signal Transduct. Target. Ther. 4, (2019).

28. Boyero, L. et al. Primary and acquired resistance to immunotherapy in lung cancer: Unveiling the mechanisms underlying of immune checkpoint blockade therapy. Cancers (Basel). 12, 1–36 (2020).
29. Mamdani, H., Matosevic, S., Khalid, A. B., Durm, G. & Jalal, S. I. Immunotherapy in Lung Cancer: Current Landscape and Future Directions. Front. Immunol. 13, 1–12 (2022).
30. Shiravand, Y. et al. Immune Checkpoint Inhibitors in Cancer Therapy. Curr. Oncol. 29, 3044–3060 (2022).
31. Paulsen, E.-E. et al. CTLA-4 expression in the non-small cell lung cancer patient tumor microenvironment: diverging prognostic impact in primary tumors and lymph node metastases. Cancer Immunol. Immunother. 66, 1449–1461 (2017).
32. Vellanki, P. J. et al. FDA Approval Summary: Nivolumab with Ipilimumab and Chemotherapy for Metastatic Non-Small Cell Lung Cancer, a Collaborative Project Orbis Review. Clin. Cancer Res. Off. J. Am. Assoc. Cancer Res. 27, 3522–3527 (2021).
33. Dagogo-Jack, I. & Shaw, A. T. Tumour heterogeneity and resistance to cancer therapies. Nat. Rev. Clin. Oncol. 15, 81–94 (2018).
34. Lv, P., Man, S., Xie, L., Ma, L. & Gao, W. Pathogenesis and therapeutic strategy in platinum resistance lung cancer. Biochim. Biophys. Acta - Rev. Cancer 1876, 188577 (2021).
35. Bou Antoun, N. & Chioni, A. M. Dysregulated Signalling Pathways Driving Anticancer Drug Resistance. Int. J. Mol. Sci. 24, (2023).
36. Meador, C. B. & Hata, A. N. Acquired resistance to targeted therapies in NSCLC: Updates and evolving insights. Pharmacol. Ther. 210, 107522 (2020).
37. Wu, J. & Lin, Z. Non-Small Cell Lung Cancer Targeted Therapy: Drugs and Mechanisms of Drug Resistance. Int. J. Mol. Sci. 23, (2022).
38. Ashrafi, A. et al. Current Landscape of Therapeutic Resistance in Lung Cancer and Promising Strategies to Overcome Resistance. Cancers (Basel). 14, (2022).
39. Frisone, D., Friedlaender, A., Addeo, A. & Tsantoulis, P. The Landscape of Immunotherapy Resistance in NSCLC. Front. Oncol. 12, 1–10 (2022).

40. Wu, B., Zhang, B., Li, B., Wu, H. & Jiang, M. Cold and hot tumors: from molecular mechanisms to targeted therapy. Signal Transduct. Target. Ther. 9, 274 (2024).
41. Jones, V. S. et al. Cytokines in cancer drug resistance: Cues to new therapeutic strategies. Biochim. Biophys. Acta - Rev. Cancer 1865, 255–265 (2016).
42. Pasini, L. & Ulivi, P. Extracellular vesicles in non-small-cell lung cancer: Functional role and involvement in resistance to targeted treatment and immunotherapy. Cancers (Basel). 12, (2020).
43. Liu, J. et al. The biology, function, and applications of exosomes in cancer. Acta Pharm. Sin. B 11, 2783–2797 (2021).
44. Wang, J., Liu, Q., Zhao, Y., Fu, J. & Su, J. Tumor Cells Transmit Drug Resistance via Cisplatin-Induced Extracellular Vesicles. Int. J. Mol. Sci. 24, (2023).
45. Mathew, M. et al. Extracellular vesicles as biomarkers in cancer immunotherapy. Cancers (Basel). 12, 1–21 (2020).
46. Xin, P. et al. The role of JAK/STAT signaling pathway and its inhibitors in diseases. Int. Immunopharmacol. 80, 106210 (2020).
47. Xue, C. et al. Evolving cognition of the JAK-STAT signaling pathway: autoimmune disorders and cancer. Signal Transduct. Target. Ther. 8, (2023).
48. Verhoeven, Y. et al. The potential and controversy of targeting STAT family members in cancer. Semin. Cancer Biol. 60, 41–56 (2020).
49. Gao, Y. et al. IFN-γ-mediated inhibition of lung cancer correlates with PD-L1 expression and is regulated by PI3K-AKT signaling. Int. J. Cancer 143, 931–943 (2018).
50. Zhang, X. et al. PD-L1 induced by IFN-γ from tumor-associated macrophages via the JAK/STAT3 and PI3K/AKT signaling pathways promoted progression of lung cancer. Int. J. Clin. Oncol. 22, 1026–1033 (2017).
51. Abdel-Rahman, O. Correlation between PD-L1 expression and outcome of NSCLC patients treated with anti-PD-1/PD-L1 agents: A meta-analysis. Crit. Rev. Oncol. Hematol. 101, 75–85 (2016).
52. Théry, C. et al. Minimal information for studies of extracellular vesicles 2018 (MISEV2018): a position statement of the International Society for Extracellular Vesicles and update of the MISEV2014 guidelines. J. Extracell. Vesicles 7, (2018).

53. Zhang, X. et al. PD-L1 induced by IFN-γ from tumor-associated macrophages via the JAK/STAT3 and PI3K/AKT signaling pathways promoted progression of lung cancer. Int. J. Clin. Oncol. 22, 1026–1033 (2017).
54. Wiechmann, A. et al. CD107a+ (LAMP-1) Cytotoxic CD8+ T-Cells in Lupus Nephritis Patients. Front. Med. 8, 1–9 (2021).
55. Chen, Z., Fillmore, C. M., Hammerman, P. S., Kim, C. F. & Wong, K. K. Non-small-cell lung cancers: A heterogeneous set of diseases. Nat. Rev. Cancer 14, 535–546 (2014).
56. Srinivas US, Tan BWQ, Vellayappan BA, Jeyasekharan AD. ROS and the DNA damage response in cancer. Redox Biol. 2019 Jul;25:101084.
57. Sabharwal SS, Schumacker PT. Mitochondrial ROS in cancer: initiators, amplifiers or an Achilles' heel? Nat Rev Cancer. 2014 Nov;14(11):709-21.
58. Zhang, Y. et al. HKDC1 promotes tumor immune evasion in hepatocellular carcinoma by coupling cytoskeleton to STAT1 activation and PD-L1 expression. Nat. Commun. 15, (2024).
59. Cerezo, M. et al. Translational control of tumor immune escape via the eIF4F–STAT1–PD-L1 axis in melanoma. Nat. Med. 24, 1877–1886 (2018).
60. Jiang, Y. et al. Reciprocal inhibition between TP63 and STAT1 regulates anti-tumor immune response through interferon-γ signaling in squamous cancer. Nat. Commun. 15, (2024).
61. Chen, M. & Wang, S. Preclinical development and clinical studies of targeted JAK/STAT combined Anti-PD-1/PD-L1 therapy. Int. Immunopharmacol. 130, 111717 (2024).
62. Padmanabhan, S., Gaire, B., Zou, Y., Uddin, M. M. & Vancurova, I. IFNγ-induced PD-L1 expression in ovarian cancer cells is regulated by JAK1, STAT1 and IRF1 signaling. Cell. Signal. 97, (2022).
63. Taniguchi, H. et al. WEE1 inhibition enhances the antitumor immune response to PD-L1 blockade by the concomitant activation of STING and STAT1 pathways in SCLC. Cell Rep. 39, (2022).
64. Freitas-Dias, C. et al. Interaction between NSCLC Cells, CD8+ T-Cells and Immune Checkpoint Inhibitors Potentiates Coagulation and Promotes Metabolic Remodeling—New Cues on CAT-VTE. Cells 13, 1–21 (2024).

65. Meissl, K. et al. STAT1 Isoforms Differentially Regulate NK Cell Maturation and Anti-tumor Activity. Front. Immunol. 11, 1–15 (2020).
66. Zhu, H. et al. Inhibition of STAT1 sensitizes renal cell carcinoma cells to radiotherapy and chemotherapy. Cancer Biol. Ther. 13, 401–407 (2012).
67. Stronach, E. A. et al. HDAC4-regulated STAT1 activation mediates platinum resistance in ovarian cancer. Cancer Res. 71, 4412–4422 (2011).
68. Zellmer, V. R. et al. Tumor-induced stromal STAT1 accelerates breast cancer via deregulating tissue homeostasis. Mol. Cancer Res. 15, 585–597 (2017).
69. Cheng, Z. hui et al. Chemokines and their receptors in lung cancer progression and metastasis. J. Zhejiang Univ. Sci. B 17, 342–351 (2016).
70. Fousek, K., Horn, L. A. & Palena, C. Interleukin-8: A chemokine at the intersection of cancer plasticity, angiogenesis, and immune suppression. Pharmacol. Ther. 219, (2021).
71. Padmanabhan, S. et al. IFNγ induces JAK1/STAT1/p65 NFκB-dependent interleukin-8 expression in ovarian cancer cells, resulting in their increased migration. Int. J. Biochem. Cell Biol. 141, 106093 (2021).
72. Du, J. et al. IL-8 regulates the doxorubicin resistance of colorectal cancer cells via modulation of multidrug resistance 1 (MDR1). Cancer Chemother. Pharmacol. 81, 1111–1119 (2018).
73. Cheng, M. et al. Histone deacetylase 6 regulated expression of IL-8 is involved in the doxorubicin (Dox) resistance of osteosarcoma cells via modulating ABCB1 transcription. Eur. J. Pharmacol. 840, 1–8 (2018).
74. Zhai, J. et al. Cancer-associated fibroblasts-derived IL-8 mediates resistance to cisplatin in human gastric cancer. Cancer Lett. 454, 37–43 (2019).
75. Milosevic, V. et al. Wnt/IL-1β/IL-8 autocrine circuitries control chemoresistance in mesothelioma initiating cells by inducing ABCB5. Int. J. Cancer 146, 192–207 (2020).
76. Korbecki, J., Barczak, K., Gutowska, I., Chlubek, D. & Baranowska-Bosiacka, I. CXCL1: Gene, Promoter, Regulation of Expression, mRNA Stability, Regulation of Activity in the Intercellular Space. Int. J. Mol. Sci. 23, 1–25 (2022).

77. Liu, G. et al. Specific chemotherapeutic agents induce metastatic behaviour through stromal- and tumour-derived cytokine and angiogenic factor signalling. J. Pathol. 237, 190–202 (2015).
78. Korbecki, J. et al. The Clinical Significance and Involvement in Molecular Cancer Processes of Chemokine CXCL1 in Selected Tumors. Int. J. Mol. Sci. 25, 1–28 (2024).
79. Sharma, B., Nawandar, D. M., Nannuru, K. C., Varney, M. L. & Singh, R. K. Targeting CXCR2 enhances chemotherapeutic response, inhibits mammary tumor growth, angiogenesis, and lung metastasis. Mol. Cancer Ther. 12, 799–808 (2013).
80. Raghuwanshi, S. K., Nasser, M. W., Chen, X., Strieter, R. M. & Richardson, R. M. Depletion of β-Arrestin-2 Promotes Tumor Growth and Angiogenesis in a Murine Model of Lung Cancer. J. Immunol. 180, 5699–5706 (2008).
81. Acharyya, S. et al. A CXCL1 paracrine network links cancer chemoresistance and metastasis. Cell 150, 165–178 (2012).
82. Li, J. et al. Tumor Cell-Intrinsic Factors Underlie Heterogeneity of Immune Cell Infiltration and Response to Immunotherapy. Immunity 49, 178-193.e7 (2018).
83. Cheng, H. Y., Su, G. L., Wu, Y. X., Chen, G. & Yu, Z. L. Extracellular vesicles in anti-tumor drug resistance: Mechanisms and therapeutic prospects. J. Pharm. Anal. 14, (2024).
84. Mullen, S. & Movia, D. The role of extracellular vesicles in non-small-cell lung cancer, the unknowns, and how new approach methodologies can support new knowledge generation in the field. Eur. J. Pharm. Sci. 188, 106516 (2023).
85. Sheta, M., Taha, E. A., Lu, Y. & Eguchi, T. Extracellular Vesicles: New Classification and Tumor Immunosuppression. Biology (Basel). 12, 1–29 (2023).
86. Buzas, E. I. The roles of extracellular vesicles in the immune system. Nat. Rev. Immunol. 23, 236–250 (2023).
87. Lundholm, M. et al. Prostate tumor-derived exosomes down-regulate NKG2D expression on natural killer cells and CD8+ T cells: Mechanism of immune evasion. PLoS One 9, (2014).
88. Fitzgerald, W. et al. A System of Cytokines Encapsulated in ExtraCellular Vesicles. Sci. Rep. 8, 1–11 (2018).

89. Wang, S. et al. Baohuoside I chemosensitises breast cancer to paclitaxel by suppressing extracellular vesicle/CXCL1 signal released from apoptotic cells. J. Extracell. Vesicles 13, (2024).
90. Wang, S. et al. XIAOPI formula inhibits chemoresistance and metastasis of triple-negative breast cancer by suppressing extracellular vesicle/CXCL1-induced TAM/PD-L1 signaling. Phytomedicine 135, (2024).
91. Wu, Y. & Song, H. A Comparative and Comprehensive Review of Antibody Applications in the Treatment of Lung Disease. Life 12, (2022).
92. Kowalski, K. Recent developments in the chemistry of ferrocenyl secondary natural product conjugates. Coord. Chem. Rev. 366, 91–108 (2018).
93. Ornelas, C. Application of ferrocene and its derivatives in cancer research. New J. Chem. 35, 1973–1985 (2011).
94. Couto, M. et al. Discovery of Potent EGFR Inhibitors through the Incorporation of a 3D-Aromatic-Boron-Rich-Cluster into the 4-Anilinoquinazoline Scaffold: Potential Drugs for Glioma Treatment. Chem. - A Eur. J. 24, 3122–3126 (2018).
95. Biegański, P. et al. Click ferrocenyl-erlotinib conjugates active against erlotinib-resistant non-small cell lung cancer cells in vitro. Bioorg. Chem. 119, (2022).
96. Ortega, E. et al. An Erlotinib gold(I) conjugate for combating triple-negative breast cancer. J. Inorg. Biochem. 203, 110910 (2020).
97. Kowalski, K., Hikisz, P., Szczupak, Ł., Therrien, B. & Koceva-Chyła, A. Ferrocenyl and dicobalt hexacarbonyl chromones - New organometallics inducing oxidative stress and arresting human cancer cells in G2/M phase. Eur. J. Med. Chem. 81, 289–300 (2014).
98. Trondl, R. et al. NKP-1339, the first ruthenium-based anticancer drug on the edge to clinical application. Chem. Sci. 5, 2925–2932 (2014).
99. An, X. et al. Oxidative cell death in cancer: mechanisms and therapeutic opportunities. Cell Death Dis. 15, (2024).
100. Ghosh, S. Cisplatin: The first metal based anticancer drug. Bioorg. Chem. 88, 102925 (2019).
101. Kciuk, M. et al. Doxorubicin—An Agent with Multiple Mechanisms of Anticancer Activity. Cells 12, 26–32 (2023).

102. Couto, M. et al. Discovery of Potent EGFR Inhibitors through the Incorporation of a 3D-Aromatic-Boron-Rich-Cluster into the 4-Anilinoquinazoline Scaffold: Potential Drugs for Glioma Treatment. Chem. - A Eur. J. 24, 3122–3126 (2018).
103. Mao, L. F. et al. Design, Synthesis, and Antitumor Activity of Erlotinib Derivatives. Front. Pharmacol. 13, 1–14 (2022).

## 8. Acknowledgements

Devo essere sincera: non ho dato per scontato di arrivare al termine di questo percorso, neanche per un momento. Eppure, eccomi qui. Il dottorato è, però, una via che non si può percorrere da soli, e io sono stata abbastanza fortunata da avere avuto accanto così tante persone da poter riempire un'intera pagina di ringraziamenti.

Il primo e fondamentale grazie va a Chiara e Asia, che mi hanno presa con loro ancora prima di questi quattro anni e mi hanno formata con pazienza e professionalità: la vostra è stata una guida rara e preziosa.

Un altro grandissimo grazie va a tutti i membri del lab, presenti e passati, il cui supporto, spesso anche extra-accademico, è stato essenziale per farmi crescere come scienziata e come persona. Grazie soprattutto a Muhlis, che mi ha conosciuta nel lontano 2018 e ha visto il meglio e il peggio di questi anni. Un grandissimo *obrigada* anche alle ragazze del lab portoghese, che mi hanno fatto sentire a casa ancora prima di mettere piede a Porto.

A Sabri, poi, devo un ringraziamento che non ha bisogno di spiegazioni. Si dice che alla fine del proprio braccio si trovi la mano di cui si ha bisogno: nel tuo caso, però, troverai sempre anche la mia.

Grazie a Bea, che è stata una presenza costante nella mia vita da ben prima del dottorato, ma soprattutto anche in barba alla Brexit: sappi che è arrivato il momento di aprire la libreria-caffè di cui parliamo da anni; quindi, lascia perdere gli inglesi e inizia a fare le valigie.

Mille volte grazie anche a Ele e Miri, con cui ho condiviso approssimativamente duecento merende, cinquecento foto di gatti e, nell'ordine, un appartamento e una residenza universitaria.

Un grazie importantissimo anche a Trouvaille, scoperta per caso e diventata ormai una seconda casa, che mi ha fatto conoscere delle persone meravigliose, disposte a leggere le atrocità per niente scientifiche che escono dalla mia penna.

E quindi, ovviamente, menzione speciale ad Ari, che scrive pure di peggio: grazie per essere l'amica che la me bambina ha sempre voluto. La stanza al CSM sarà piccolina ma ce la faremo andare bene.

Grazie a Marti, che crede in me più di quanto faccia io stessa, e che riesce a trasformare anche le brutte serate in un pigiama party. La vita con te è una storia scritta a quattro a mani, e non potrei desiderare un co-autore migliore.

Infine, ringrazio la mia famiglia per avermi supportato senza remore nell'ennesima tappa universitaria, e in particolare mio nonno, che ancora mi chiede se il dottorato mi farà finalmente diventare professore ordinario.
Ma soprattutto grazie a mia sorella, che è presente dove la distanza me lo impedisce: nulla di quello che fai è scontato, e io l'apprezzo più di quanto queste parole sulla carta possano esprimere.